chemistry

MDPI

Review

Coumarin Derivatives as Inhibitors of Pathological Protein Aggregation, Mechanistic Basis of β-Sheet Intercalation, Structure–Activity Relationship, and Multi-Target Therapeutic Design—A Critical Review of the Computational and Biophysical Evidence

Huda Masri

Faculty of Pharmacy, Arab American University, Jenin 2000027, Palestine; huda.masri@aaup.edu

Abstract

Natural coumarins are a structurally privileged group of bioactive benzopyranone lactones widely spread across the *Apiaceae*, *Rutaceae*, and *Leguminosae* families, and hold significant potential as inhibitors of pathological protein aggregation in Alzheimer's disease, Parkinson's disease, and type 2 diabetes mellitus. The fully planar, rigid bicyclic structure of the coumarin nucleus (~3.4–3.5 Å thickness) is geometrically compatible with intercalative π–π stacking with aggregation-nucleating aromatic residues, including Phe19 of Aβ(1–42), providing a mechanistically coherent pharmacophoric basis for anti-aggregation activity according to computational and indirect biophysical evidence. This review critically evaluates the peer-reviewed literature on naturally occurring coumarins and their synthetic derivatives as candidate β-sheet intercalators, with analysis of SAR at C-3 to C-8 positions; multi-target-directed ligand designs with dual activities of inhibiting AChE, BACE-1, GSK-3β, and MAO-B, and as blood–brain barrier-penetrating neuroprotective agents validated in cellular and rodent models. The critical analysis identifies the translational gap between in vitro IC_{50} values and attainable brain drug concentrations as the primary pharmacological obstacle. It identifies the absence of systematic investigation of coumarin against IAPP, a directly relevant amyloid target in metabolic neurodegeneration, as the most significant unmet research priority in the field.

Keywords: coumarin; amyloid aggregation; β-sheet intercalation; Alzheimer disease; multi-target-directed ligands; π–π stacking; structure–activity relationship; α-synuclein; tau protein

Academic Editor: Juan B. Rodriguez

Received: 12 June 2026
Revised: 30 June 2026
Accepted: 1 July 2026
Published: 3 July 2026

1. Introduction

1.1. The Unmet Clinical Need: Amyloid-Driven Proteopathies

Proteopathies are disorders arising from pathological protein folding and aggregation; they are a mechanistically coherent class of diseases that share the common pathogenic feature of self-assembly of misfolded proteins into well-ordered, β-sheet-rich fibrillar aggregates, which are universally referred to as amyloid. The global burden of these disorders is substantial; more than 55 million people are currently living with dementia worldwide, of which 60–70% is caused by Alzheimer's (AD); approximately 10 million individuals are living with Parkinson's disease (PD); and more than 537 million adults have T2DM, in which islet amyloid polypeptide (IAPP) plays a pathogenic role in a significant

subset [1–3]. Crucially, no currently approved pharmacological agent completely modifies pathology in any of these diseases. Existing approved drugs provide mostly symptomatic relief; in the case of the recently approved anti-Aβ monoclonal antibodies, clinical benefit is limited and accompanied by a substantial burden of adverse events, such as amyloid-related imaging abnormalities (ARIA) [4].

This sustained record of clinical failure over 30 years of drug development has increasingly driven the recognition of single-target approaches and the need for small molecules that can intercept the aggregation cascade with the requisite level of mechanistic selectivity and CNS penetration for neuroprotection.

Most data on inhibitor design come from the molecular pathology of AD. According to the amyloid cascade hypothesis, successive processing of amyloid precursor protein (APP) by the enzymes β-site amyloid precursor protein cleaving enzyme-1 (BACE-1) and γ-secretase yields Aβ peptides (most commonly the 40-residue Aβ40 and the more aggregation-prone Aβ42 that self-associate via a nucleation-dependent polymerization mechanism to form soluble oligomers, protofibrils, and, finally, mature fibrillar deposits [4]. Meanwhile, the phosphorylation of microtubule-associated protein tau by enzymes such as Cdk5, GSK-3β, and JNK leads to its detachment from microtubules, formation of paired helical filaments (PHFs), and insolubilization into neurofibrillary tangles (NFTs) [5]. The key recognition that soluble oligomers, as opposed to mature fibrils, are the primary toxic species in both Aβ and tau pathology has profoundly shifted the target for the design of effective inhibitors, intending to inhibit initial events in the nucleation step and disrupt pre-fibrillar intermediates, rather than simply blocking the elongation of mature fibrils [4,6]. This shift in mechanism has implications for how anti-aggregation IC_{50} values are interpreted and how the in vitro Thioflavin T (ThT) assays should be determined.

In this context, the coumarin scaffold (2H-1-benzopyran-2-one) presents an intriguing pharmacophoric framework for the design of anti-aggregation drugs. Coumarins are naturally occurring benzopyranones widely occurring in the plant kingdom (predominantly in *Apiaceae*, *Rutaceae* and *Leguminosae*), encompassing the anticoagulant warfarin, the antibiotic novobiocin, and the vasodilator coumermycin [7,8]. In terms of neurodegenerative pharmacology, the coumarin nucleus offers a unique combination of structural features: planarity to insert into β-sheets, synthetic tractability to systematically explore structure–activity relationships (SARs) across six substitution positions, intrinsic lipophilicity consistent with brain penetration, and a natural product origin that presages inherent biocompatibility. The focus of this review is to evaluate whether these structural advantages translate to therapeutically relevant anti-aggregation activity at pharmacologically relevant concentrations.

1.2. Literature Search Methodology

A literature search of the PubMed/MEDLINE, Scopus, and Web of Science databases was conducted from 2010 to 2025. Major Boolean search terms were (“coumarin” OR “benzopyranone” OR “chromone”) AND (“amyloid aggregation” OR “protein aggregation” OR “β-sheet” OR “fibril formation”); (“coumarin”) AND (“Alzheimer” OR “tau” OR “alpha-synuclein” OR “IAPP”); (“coumarin”) AND (“blood–brain barrier” OR “MTDL” OR “multi-target” OR “neuroprotection”); and (“coumarin”) AND (“molecular docking” OR “SAR” OR “structure–activity”). Supplementary searches focused on specific biological targets: AChE, BuChE, BACE-1, GSK-3β and MAO-B. Selection criteria: (i) original or review papers in the English language; (ii) explicit investigation of the coumarin/benzopyranone derivatives against biochemically defined protein aggregation targets (ThT fluorescence, transmission electron microscopy (TEM), circular dichroism (CD) spectroscopy, photo-induced cross-linking of unmodified proteins (PICUP), or other equivalents); and (iii) publication of

quantitative biological results. Articles with only computational predictions were excluded, unless the authors presented mechanistic information not accessible via experiments. A total of 91 references are cited. Preference was given to mechanistic studies, SAR studies, and those that include in vitro, cell, or animal-based studies.

1.3. Scope and Organization of the Review

This review advances the existing literature on coumarin anti-aggregation drugs in three key ways. First, it provides a critical appraisal of the evidentiary status of the β-sheet intercalation model throughout the literature of coumarins, distinguishing the computational support (docking, MD simulation, and DFT) from the direct structural evidence and drawing to light the cryo-EM and NMR validation gap as the most relevant unmet methods in the field. Second, it conducts a quantitative assessment of the brain-exposure gap, which has not yet been performed on any previous coumarin review, by integrating physicochemical and in vitro permeability data to estimate the free brain concentration shortfall relative to anti-aggregation IC_{50} values of published coumarin MTDLs and approved drugs. Third, it points to IAPP as a structurally motivated, pharmacologically validated, almost unexplored target for the coumarin scaffold and suggests this as the top priority future path forward for the field, supported by the recent availability of near-atomic IAPP cryo-EM structures and the precedent of small-molecule IAPP modulation. These specific contributions differentiate this review from previous coumarin anti-aggregation reviews, which generally were descriptive SAR catalogs, lacking both the critical pharmacokinetic analysis and assessment of assay interference or disease-gap identification offered here.

Section 2 discusses the structure and physicochemical rationale of the coumarin scaffold (Figure 1 provides a chemical structure with numbered positions). Section 3 addresses the biological mechanism of β-sheet-oligomerization inhibition by coumarins, focusing on the intercalation mechanism (Figure 2 shows a schematic representation of the suggested binding mode). Section 4 provides a full, critical SAR analysis. Section 5 discusses MTDL strategies with some caveats for non-human enzyme systems. Section 6 deals with PK optimization. Section 7 reviews applications to disease-relevant amyloids. Section 8 provides a computational analysis. Sections 9–11 present the Discussion, Conclusion, and Future Prospects, respectively.

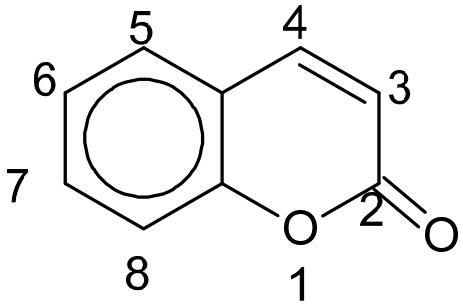

Figure 1. Chemical structure of the coumarin (2H-1-benzopyran-2-one) scaffold standard numbering of substitution positions (C-3 THROUGH C-8). The C-2 carbonyl and C-3/C-4 double bond are indicated. The figure was prepared by the author using ACD/ChemSketch 2021.2.0 (freeware).

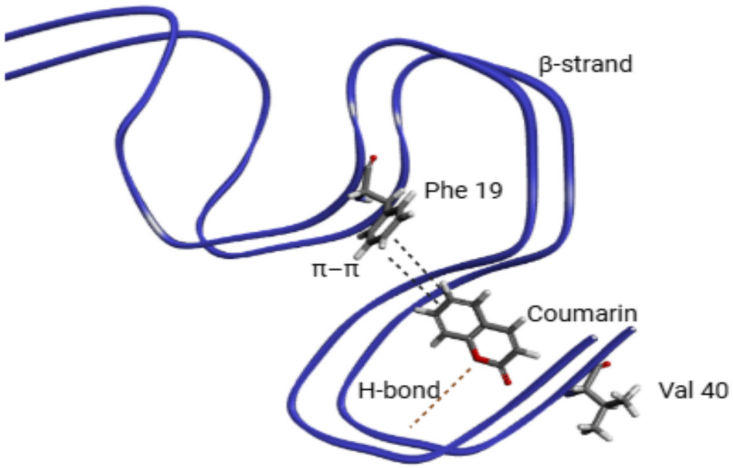

Figure 2. Schematic representation of coumarin intercalation into the Aβ(1–42) fibril inter-sheet groove. (A) Two β-strands (blue ribbons) with Phe19 and Val40 side chains shown as sticks. (B) Coumarin (gray) inserted between β-strands, with π–π stacking to Phe19 (dashed lines), hydrophobic contacts to Val40, and hydrogen bonding from the C-2 carbonyl (red) to backbone NH donors. This figure is an original schematic illustration prepared by the author using BioRender Created in BioRender. t, H. (2026) https://BioRender.com/5g2mfu8.

2. The Coumarin Scaffold: Molecular Architecture and Physicochemical Rationale

2.1. Ring Geometry, Electronic Profile, and Interaction Potential

The coumarin ring system is a planar and rigid bicyclic system where all atoms are sp^2-hybridized, with a benzene ring fused to an α,β-unsaturated δ-lactone at the 3,4-position. This results in a completely planar ring system with a thickness of 3.4–3.5 Å, which corresponds precisely to the interstrand distance of amyloid β-sheets (4.7 Å interstrand; 10–11 Å inter-sheet). This geometric compatibility represents a necessary, though not sufficient, precondition for intercalation. Computational models suggest that the coumarin ring can adopt an orientation within the inter-sheet groove that maximizes π-orbital overlap with aromatic side chains of fibril-forming residues; however, this insertion mode has not yet been confirmed by direct structural evidence such as cryo-EM co-complexes or solid-state NMR [9,10]. The C-3/C-4 double bond offers an electron-deficient π-system that can participate in charge-transfer π–π stacking with the electron-rich aromatic side chains of Phe19, Phe20, and Tyr10 of Aβ, Phe23 of IAPP, and the phenylalanine residues of α-synuclein's non-amyloid component (NAC) region [11,12].

The C-2 carbonyl group induces polarization of the aromatic system, which is a pharmacophoric feature of major significance that sets the coumarin scaffold apart from polycyclic aromatic hydrocarbons. The carbonyl oxygen is negatively charged at the B3LYP/6-311+G** DFT level (Mulliken charge −0.47 e), making it an effective hydrogen bond acceptor that forms directional H-bonds with NH donors of β-strand residues [13]. This bifunctional capacity of π-stacking and H-bonding with the carbonyl generates a multivalent non-covalent binding mode of an unusual fit with the repetitive, geometrically regular architecture of amyloid fibrils. These binding modes are of similar mechanistic character to those of the known amyloid diagnostic dyes thioflavin T (ThT) and Congo red, which bind amyloids through their planar aromatic geometry; the structural similarities between the coumarin pharmacophore and these dyes are not superficial but facilitate a compelling mechanistic understanding of anti-aggregation activity that precedes and informs the experimental literature [9,14].

The structural basis of coumarin interaction with amyloid β fibrils is illustrated in Figure 2. The model represents adjacent β-strands forming an inter-sheet groove that

accommodates the planar coumarin scaffold. Owing to its rigid, π-conjugated benzopyranone core, coumarin inserts between β-strands in a geometry compatible with interstrand spacing characteristic of amyloid β-sheets. Within this confined environment, stabilization is achieved through multiple non-covalent interactions, including π–π stacking with the aromatic side chain of Phe19, hydrophobic contacts with Val40, and hydrogen bonding between the coumarin C-2 carbonyl group and backbone amide (NH) donors. Collectively, these interactions support a plausible intercalative binding mode that may contribute to fibril stabilization or modulation of aggregation dynamics.

Regarding physicochemical properties, unsubstituted coumarin (MW 146.15 Da; logP 1.39; TPSA 26.3 $Å^2$) inherently meets CNS drug-like parameters with substantial room for synthetic elaboration. Its small molecular structure allows it to be explored across five major substitution positions, C-3, C-4, C-5, C-6, C-7, and C-8, without violating Lipinski criteria, and systematic tuning of lipophilicity, hydrogen bond capacity, molecular weight, and polar surface area is possible [7,15]. This chemical tractability has practical significance for lead optimization because substitution across five major positions can be explored while maintaining compliance with CNS drug-like physicochemical parameters, enabling systematic tuning of potency, selectivity, and pharmacokinetic properties without the constraints that limit more complex natural product scaffolds.

2.2. Comparison with Related Polyphenolic Inhibitors

Coumarins share structural features with other classes of polyphenolic amyloid inhibitors; curcumin, epigallocatechin-3-gallate (EGCG), resveratrol, quercetin, and baicalein are all based on a planar aromatic system to engage fibrils. However, a direct mechanistic comparison requires attention to the experimental conditions under which each compound was evaluated, as these are rarely standardized across studies.

Curcumin prevents Aβ fibrillation by π-stacking of its dicinnamoylmethane system with aromatic Aβ residues, with DFT-computed energies of −8.2 to −12.4 kcal/mol for interactions with Phe19, Phe20, and Tyr10 [13]. These values are numerically higher than those computed for coumarin-Phe19 interactions (−5.8 kcal/mol gas phase; −3.2 kcal/mol implicit water) [13], suggesting that, on a single-interaction basis, curcumin engages the aromatic fibril surface more strongly than the unsubstituted coumarin core. However, this comparison is confounded by differences in the computational methods used across studies (B3LYP/6-311+G for curcumin versus MP2/6-311+G** for coumarin, the absence of solvation corrections in some curcumin calculations, and the fact that potency in cell-free aggregation assays reflects a thermodynamic balance across multiple interaction modes rather than a single π-stacking event). Furthermore, the flexible, non-planar geometry of the curcumin in an aqueous solution, in which the di-keto tautomer predominates, will substantially reduce its intercalation efficiency relative to its theoretical maximum, an advantage that the rigid planar coumarin scaffold retains across solvent conditions. These differences in conformational behavior are not apparent from computed gas-phase interaction energies alone, and direct head-to-head comparison under identical assay conditions has not been reported for coumarin and curcumin. In addition, curcumin is infamously metabolically unstable, whereby the oral bioavailability is estimated at the lowest 1% in humans because of rapid glucuronidation, sulfation, and reduction [8,16]. Coumarins can be oxidized by CYP at C-3 and C-4 but have much more favorable CYP metabolism and in vivo efficacy of corresponding endpoints [17–19].

EGCG presents a mechanistically distinct comparator; the polyphenolic catechol rings of EGCG can produce potent inhibition, including disaggregation of pre-formed fibrils by non-specific binding to surfaces rather than intercalation, and extend non-selectively across at least 14 structurally diverse amyloidogenic proteins [20]. Such mechanistic promis-

cuity makes EGCG an unsuitable selective chemical probe and makes its development therapeutically very difficult. Coumarins, having a smaller and geometrically defined pharmacophore, have significantly better chances of target selectivity due to systematic manipulation of the SAR. Even this selectivity argument, though intuitively strong, is not currently adequately substantiated by experimental evidence: experiments of systematic comparative SAR analysis of coumarins with different substrates of amyloid under the same assay conditions have not been conducted, and this is a fundamental weakness in the evidence base that must be explicitly stated before making any claims of selectivity.

3. Molecular Mechanism of Coumarin-Mediated Inhibition of β-Sheet Assembly

3.1. The Cross-β Architecture as a Structural Target for Interaction

Amyloid fibrils adopt a hierarchical structural organization that defines the binding sites accessible to small-molecule inhibitors with considerable precision. β-Strands, typically 4–8 residues in length, run perpendicular to the fibril axis and hydrogen-bond laterally to form β-sheets; multiple β-sheets then stack via hydrophobic inter-sheet contacts, creating the cross-β architecture that is the defining hallmark of all amyloid fibrils regardless of primary sequence. For Aβ(1–42), solid-state NMR and cryo-EM studies have resolved this architecture with atomic detail: the peptide adopts an S-shaped fold comprising three β-strands (residues 12–18, 24–32, 36–40), with the inter-sheet interface formed by the hydrophobic groove flanked by Leu17, Val18, Phe19, Gly38, Val39, and Val40 [21]. This groove—approximately 6 Å wide and 4 Å deep—has been identified across multiple independent docking and MD simulation studies as the computationally preferred locus for coumarin binding, though experimental structural validation of this predicted binding site is currently absent [22–24].

The mechanistic case for aromatic π-stacking as a driver of amyloid self-assembly—and therefore as a tractable target for inhibition—was articulated by Gazit, who demonstrated that aromatic residues are disproportionately represented in amyloidogenic peptide segments across a diverse set of proteins and proposed that inter-residue π–π interactions provide directional, energetically favorable driving forces for fibril nucleation [11]. This hypothesis was directly validated for IAPP by experimental studies demonstrating that electron-withdrawing substituents on the Phe23 aromatic ring substantially inhibit $hIAPP_{22–29}$ fibril formation by reducing π-electron density and thus π-stacking propensity [12]. The parallel implication that electron-rich planar aromatic inhibitors can competitively occupy aromatic interaction sites within forming fibrils provides the mechanistic rationale for the coumarin anti-aggregation strategy.

3.2. Computational Evidence of π–π Stacking at Phe19 and Val40

The computational evidence for coumarin intercalation at the Phe19–Val40 inter-sheet groove is substantial but demands critical appraisal before mechanistic conclusions are drawn. Molecular docking of nine natural coumarins from *Toddalia asiatica* against the ssNMR-derived $Aβ_{1–42}$ fibril structure consistently identified π–π interactions with Phe19 and π–σ interactions with Val40 as the dominant binding contacts, with calculated binding energies of −7.0 to −9.2 kcal/mol [23]. Hashemi et al. used MD simulations up to 100 ns to show that coumarin treatment was associated with a reduction in mean β-strand content per Aβ oligomer, as well as increased Cα-Cα distances between Phe19 and Val40 by a factor of about 0.8 Å, consistent with disruption of inter-sheet contacts, though these findings await confirmation by direct structural methods [22]. At the MP2/6-311+G** level, the π-stacking interaction energy between the coumarin ring and a Phe side chain model has been quantified using DFT to be −5.8 kcal/mol in the gas phase and −3.2 kcal/mol in

an implicit water model, a thermodynamically significant value and comparable to the numbers obtained for curcumin [25–27].

However, there is a critical qualification that must accompany the body of computational evidence reviewed in this section. All docking and MD studies of coumarin-Aβ interactions are based on only a few structures of static Aβ fibrils, and the resulting data cannot be generalized to the full structural diversity of Aβ polymorphs confirmed by cryo-EM or to the ex vivo fibril structures derived from AD patient brain tissue, which are structurally different from the in vitro recombinant fibrils.

The Phe19–Val40 binding mode identified by docking is a computational prediction that, while mechanistically and indirectly supported by biophysical measurements, has not been confirmed by any direct structural method, including cryo-EM density maps of coumarin–fibril complexes, solution-phase STD-NMR of coumarin binding to fibrillar Aβ, or solid-state NMR chemical shift perturbations. Until these data become available, the intercalation model should be given in the form of a well-supported working hypothesis rather than in the form of a structural fact. Throughout this review, mechanistic conclusions made on the basis of docking and MD data will be considered to be applicable to this qualification.

3.3. Hydrogen Bonding, Hydrophobic Contacts, and the Multivalent Binding Mode

Beyond π-stacking, experimental biophysical data have shown that a multivalent binding mode can be employed, in which the coumarin carbonyl and ring hydroxyl groups are directionally hydrogen-bonded to fibril surface residues, and the C-4, C-6, and C-8 hydrophobic groups make van der Waals contacts within the inter-sheet groove. In β-lactoglobulin (β-lg) model aggregation studies, fluorescence quenching analyses using Stern–Volmer analysis indicated static quenching of protein intrinsic fluorescence, consistent with formation of a stable ground-state coumarin–protein complex at a single high-affinity site (Ka ~10^4–10^5 M^{-1}) [28]. CD spectroscopy demonstrated that coumarin binding shifted the secondary structure content of β-lg toward higher α-helical and lower β-sheet proportions even at sub-stoichiometric concentrations, indicating stabilization of the native protein conformation against the β-sheet-rich intermediate that initiates aggregation. The 8-hydroxy derivative was the most effective, attributable to the additional H-bond donation from the C-8 hydroxyl to a polar residue at the hydrophobic binding site [26,27].

A fundamental limitation of β-lg and HEWL as model systems must be acknowledged here and applied consistently through all subsequent mechanistic interpretations. Neither is an intrinsically disordered protein (IDP): aggregation in both systems is induced by thermal denaturation rather than by the nucleation-dependent polymerization mechanism operative in AD, PD, and T2DM. The thermodynamic driving forces for aggregation and the energetic landscape that an inhibitor must navigate are qualitatively different in IDP-based amyloid systems. Binding constants measured against native globular proteins cannot be extrapolated to Aβ, tau, or α-synuclein aggregation inhibition, and this distinction is insufficiently emphasized in many published coumarin studies [25,28]. Accordingly, wherever HEWL or β-lg data are cited in the SAR analysis or in the mechanistic discussion, they are presented as mechanistic proxies providing structural plausibility only, not as evidence of activity against disease-relevant targets. The field would benefit substantially from prioritizing mechanistic characterization in amyloidogenic peptide systems ($Aβ_{16–22}$, $IAPP_{22–29}$) for which cryo-EM fibril structures are available and ligand binding can be assessed by solution NMR.

3.4. Mechanistic Basis of Interference with Nucleation and Elongation Kinetics

The nucleation-dependent polymerization model of amyloid formation encompasses at least three kinetically distinguishable phases: primary nucleation (formation of ordered nuclei from disordered monomers), secondary nucleation (fibril surface-catalyzed formation of new nuclei from monomers), and elongation (monomer addition to fibril ends). Mathematical modeling of ThT fluorescence kinetic curves can, in principle, deconvolve inhibitor effects on these phases; such analysis is of the utmost therapeutic relevance because secondary nucleation is the dominant source of new nuclei under physiological conditions, and compounds that inhibit this process are predicted by kinetic models to be disproportionately more effective at reducing total amyloid burden than elongation-only inhibitors [9]. Ono and colleagues demonstrated that derivatization of the coumarin aromatic center markedly shifts the point of inhibitory intervention: unsubstituted coumarin acts predominantly at the elongation phase, while benzothiazole- and triazole-functionalized derivatives, whose substituents replicate functional groups present in amyloid-binding dyes, shift activity toward the nucleation phase [9]. This mechanistic heterogeneity has critical implications for lead selection and is largely absent from the current coumarin anti-aggregation literature.

Amide-linked coumarin scaffolds bearing diverse phenolic substituents have demonstrated inhibition of both α-synuclein and tau oligomerization by PICUP assay and mature fibril formation by ThT and TEM at 100 μM in vitro [29]. The concurrent activity against structurally distinct amyloidogenic proteins at identical concentrations suggests a mechanism dependent on the coumarin pharmacophore rather than sequence-specific recognition, which is an interpretation that requires validation by competitive binding studies and site-directed mutagenesis of proposed binding residues. Disaggregation of pre-formed HEWL fibrils by 4-methylcoumarin and 4-methylthiocoumarin was confirmed by TEM, showing conversion of fibrillar to amorphous morphologies, and by CD spectroscopy, demonstrating β-sheet content loss [26]. As discussed in Section 3.3, HEWL is a globular model protein whose aggregation mechanism is mechanistically distinct from IDP-based amyloidogenesis; this finding is therefore presented as a mechanistic proxy for disaggregation activity rather than direct evidence of efficacy against disease-relevant fibrils. Whether this disaggregation activity extends to thermodynamically more stable, disease-relevant Aβ or tau fibrils has not been established.

3.5. Metal Chelation as a Complementary Anti-Aggregation Mechanism

An underappreciated dimension of the coumarin anti-aggregation mechanism involves metal ion chelation. Abnormal homeostasis of Cu^{2+}, Zn^{2+}, and Fe^{3+} has a well-established role in facilitating Aβ aggregation, tau hyperphosphorylation, and oxidative stress in brain tissue in AD. Cu^{2+} and Zn^{2+} bind Aβ at His6, His13, His14, and Asp1, stimulating oligomerization and structurally aberrant, especially toxic aggregates. Coumarin derivatives with catechol or 8-hydroxyquinoline-like motifs have metal-binding capacity that can, independent of direct fibril binding, potentially bind pro-aggregant metal ions [30–32]. The 3-acetyl coumarin thiosemicarbazone was able to inhibit Aβ(1–42) aggregation by 80 percent compared to 52 percent with the parent molecule [30]. This is probably due to a combination of effects: the coumarin nucleus intercalates the 3-acetyl group by binding to the metal, while the thiosemicarbazone nitrogen atoms chelate.

The enhanced inhibitory activity of the thiosemicarbazone derivative compared to the parent compound is consistent with, but does not prove, a dual mechanism involving both β-sheet intercalation by the coumarin core and metal chelation by the thiosemicarbazone nitrogen donors. This interpretation is inferential; given that thiosemicarbazone-containing compounds are recognized PAINS scaffolds, the enhanced inhibitory effect requires or-

thogonal experimental validation (TEM, CD, and metal-free competitive binding assays) before any mechanistic assignment can be made with confidence. The anti-aggregation mechanisms described above are integrated schematically in Figure 3.

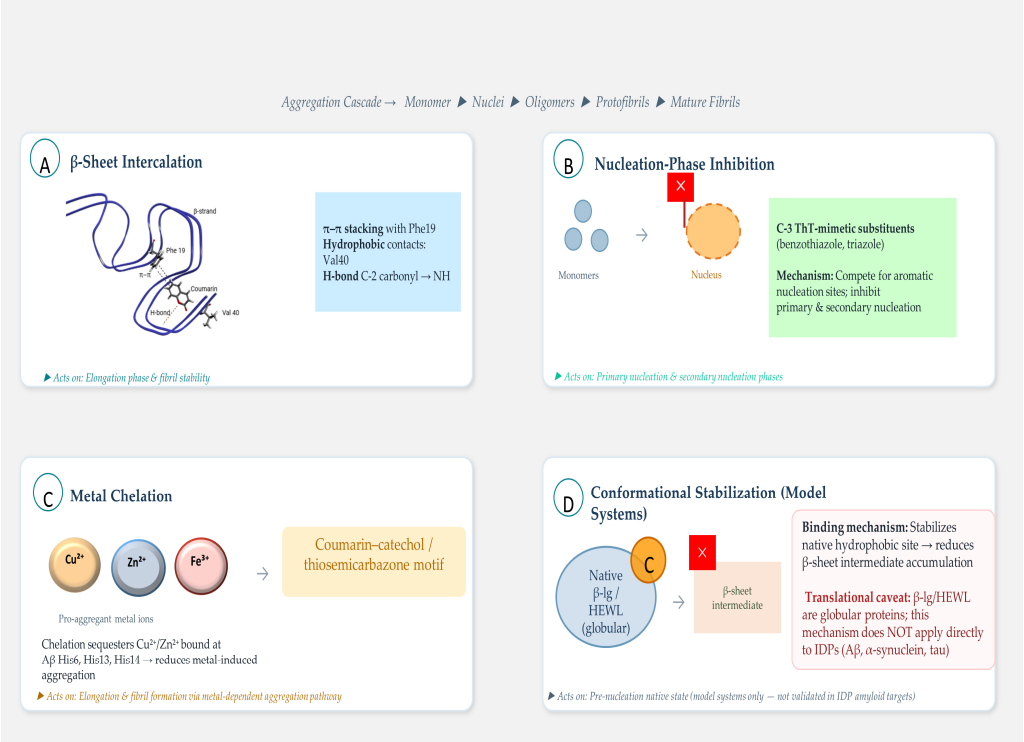

Figure 3. Proposed schematic overview of the major anti-aggregation mechanism of coumarin derivatives. The figure shows a diagram aligned with the stages of the nucleation-dependent polymerization model. (**A**) β-sheet intercalation: the planar coumarin bicyclic core inserts into the inter-sheet groove of Aβ(1–42) fibrils, with π–π stacking at Phe19, hydrophobic contacts at Val40, and hydrogen bonding from the C-2 carbonyl to backbone NH donors. (**B**) Nucleation-phase inhibition: coumarin derivatives bearing ThT-mimetic substitution (benzothiazole, triazole at C-3) are shown interacting with early stage oligomeric nuclei, disrupting ordered nucleus formation. (**C**) Metal chelation: coumarin derivatives bearing catechol or thiosemicarbazone motifs sequester Cu^{2+}, Zn^{2+}, and Fe^{2+}, preventing metal-induced Aβ aggregation at His6/His13/His14. (**D**) Conformational stabilization: binding to the native hydrophobic site of globular model proteins (β-lg, HEWL) stabilizes the native fold against β-sheet-rich intermediate states; a translational caveat notation indicates that this mechanism is not directly applicable to IDP targets. This figure is prepared by the author using Microsoft PowerPoint (Microsoft Corporation, Redmond, WA, USA).

4. A Systematic Analysis of the Structure–Activity Relationship

The considerable body of SAR data collected on coumarin derivatives across a variety of biological targets allows a pharmacophore map of useful resolution to be built. A critical methodological caveat applies to all ThT-derived anti-aggregation data discussed in this section, as fluorescent coumarin derivatives are documented to cause ThT assay interference through inner filter effects, fluorescence augmentation, and autofluorescence artefacts, all of which can produce false-positive inhibition readouts [33,34]. The study by Masroor et al. provides a direct example of a highly fluorescent coumarin derivative initially classified as an inhibitor whose activity was subsequently shown to arise from ThT signal suppression rather than genuine fibril inhibition [33]. Accordingly, all IC_{50} or percentage inhibition values cited below should be understood as requiring orthogonal validation by TEM, CD spectroscopy, DLS, or native PAGE before they can be accepted as genuine, structure-specific anti-aggregation effects. Where such orthogonal validation has

been performed, it is noted explicitly. Where it has not, the data are treated as preliminary and mechanistically inconclusive.

The analysis is grouped by position of substitution below, with a special focus on conflicting data, mechanistic interpretations that are still debated and systematic constraints that restrict interpretation of reported potency values.

4.1. C-3 Position: The Primary Site for Anti-Aggregation Elaboration

The C-3 position is the most pharmacologically productive site of anti-aggregation activity modulation. Replacement with a carboxamide linker at C-3 to enable the attachment of the coumarin nucleus to a wide range of phenolic functional groups creates scaffolds that can target 3-fold aggregation of alpha-syn and tau and retain the molecular geometry needed to bind β-sheets [29]. Mechanistically, this is explained by the lengthening of the molecular conjugated system via the amide bond to the pendant phenolic ring, which results in a larger planar surface area that increases π-orbital overlaps during intercalation. A systematic screening of natural coumarins in nine *Toddalia asiatica* derivatives illustrated that the π–π and π-σ interactions of Phe19 and Val40, respectively, were conserved in all derivatives regardless of C-3 substitution in docking simulations, establishing the bicyclic core as the major pharmacophoric component in the computational models [23]. It is important to emphasize that such consistency across a docking study is not experimental proof that the binding mode is preserved in solution and/or fibrillar contexts with the individual C-3 substituted compounds, but rather the geometric constraints of the docking target.

Introduction of thiosemicarbazone functionality at the C-3 acetyl group produced an 80% inhibition of Aβ(1–42) aggregation compared to 52% for the unmodified parent 3-acetylcoumarin [30]. The mechanistic basis for this enhancement likely involves the extended H-bond network introduced by the thiosemicarbazone –NH–C(=S)–NH_2 group, supplemented by the metal chelation capacity discussed in Section 3.5. The PAINS caveat noted above applies with particular force here and must be addressed experimentally before the reported 80% inhibition is accepted as a structure-specific effect.

4.2. C-4 Position: Hydrophobic Pocket Engagement at Val40

Substituents at C-4 primarily modulate hydrophobic contact with the Val40-containing inter-sheet pocket. Methyl and phenyl groups at C-4 consistently augment anti-aggregation potency in docking studies, with increased van der Waals contact energy attributed to more favorable packing against Val40, Gly38, and Val39 [23,35,36]. The notopterol-derived coumarin bearing a strategic C-4 substitution characterized by Liu and colleagues demonstrated AChE inhibition at IC_{50} = 1.313 μM with a selectivity index of 24.6 over BuChE, and BACE-1 inhibition at IC_{50} = 1.227 μM, alongside confirmed PAMPA-BBB permeability and acceptable acute toxicity profiles assessed against HepG2, HL-7702, and SH-SY5Y cell lines [35,36]. The inclusion of cytotoxicity assessment against both cancer and normal hepatic cell lines strengthens the therapeutic relevance interpretation.

4.3. C-7 Position: A Key Determinant of Cholinesterase Selectivity and BBB Permeability

The C-7 position has emerged as a pharmacologically versatile locus, with substituents critically influencing AChE/BuChE selectivity, MAO-B inhibitory activity, BBB permeability, and anti-aggregation potency. The AChE-inhibitory activity of aromatic amine substituents at C-7, especially piperazinyl, morpholinyl and pyrrolidinyl groups, has been consistently reported to be enhanced; the mechanism rationale behind this effect is π-cation interaction of the protonated nitrogen of the pendant amine groups and the aromatic side chain of Trp279 at the peripheral anionic site (PAS) of AChE combined with steric occupation of the catalytic anionic site (CAS) by the coumarin nucleus [37–39].

A recent systematic review of 7-hydroxycoumarin derivatives found that C-7, C-3, and C-4 substitutions have the strongest effect on pharmacological potency and selectivity, with multiple of the derivatives having sub-micromolar-nanomolar AChE and MAO-B inhibitory activity equivalent to approved drugs [40].

There is a vital point that must be stated explicitly: most studies that report C-7-substituted coumarin AChE inhibitors employ electric eel (eEL) AChE instead of human recombinant hAChE, and the selectivity indices are often determined against eEL BuChE instead of human BuChE. Given that eEL AChE and hAChE differ substantially in PAS composition, such that hAChE contains Asp72 at a position occupied by Glu73 in eEL AChE, altering the electrostatic contacts that govern PAS-binding substituent affinity and can differently affect potency for compounds whose binding is driven by electrostatic or H-bond interactions at the PAS [41]. Potency data generated with non-human enzyme preparations therefore cannot be applied directly to therapeutic prediction, and this limitation afflicts the majority of the published coumarin cholinesterase inhibitor literature and is insufficiently acknowledged in summary reviews of coumarin MTDL candidates.

With respect to BBB permeability, hydroxyl groups at C-7 introduce hydrogen bond donors that elevate TPSA and reduce passive transcellular diffusion. Methyl ether masking of phenolic hydroxyls consistently improves PAMPA-BBB permeability without proportionally reducing target affinity, since methoxy groups retain electron donation to the aromatic ring while eliminating H-bond donation. The introduction of trifluoromethyl groups, particularly at C-3, produced a five-fold improvement in BACE-1 inhibition alongside maintained BBB permeability in 4-trifluoromethyl-coumarin hybrids, attributable to the strong electron-withdrawing effect of CF_3 improving binding to the aspartate dyad of the BACE-1 active site [42].

4.4. C-6 and C-8 Positions: Chain Length, Antioxidant Activity, and Aggregation Selectivity

Long alkyl chains at C-6 enable dual-binding site engagement of AChE, simultaneously occupying CAS and PAS through a bivalent mechanism mechanistically analogous to bis-tacrine dimers [43,44]. The optimal chain length for this dual-site engagement was identified as C6–C8 in the *Toddalia asiatica* series, with phellopterin demonstrating the most potent multifunctional activity [23].

The C-8 position has a particular relationship with antioxidant and anti-aggregation properties: the 8-hydroxy substitution creates a catechol-like motif conferring radical scavenging properties through ortho-phenol electron donation. In the β-lg model system, the 8-hydroxy derivative demonstrated the most effective inhibition of thermally induced aggregation, attributable to the additional H-bond donation from the C-8 hydroxyl to a polar residue at the hydrophobic binding site [28]. As noted in Section 3.3, β-lg is a globular protein whose aggregation mechanism is mechanistically distinct from IDP amyloidogenesis; these findings therefore support a plausible H-bonding role for the C-8 hydroxyl in a structured hydrophobic environment but do not constitute evidence for equivalent activity against Aβ, α-synuclein, or tau fibrils separately. 7,8-Dihydroxy-4-methylcoumarin (DHMC) demonstrated neuroprotection against glutamate toxicity in hippocampal HT-22 cells by inhibiting glutathione depletion and ROS generation and reduced infarct volume in neonatal rat hypoxia/ischemia models—providing rare in vivo evidence for the neuroprotective relevance of the 8-hydroxy coumarin pharmacophore through an antioxidant rather than anti-aggregation mechanism [45].

4.5. Ring Fusion and Hybrid Scaffolds: Expanding the π-System

Ring fusion strategies that expand the planar aromatic surface of the coumarin nucleus represent the most structurally ambitious approach to enhanced intercalation effi-

ciency. Coumarin–triazole hybrids have demonstrated simultaneous inhibition of AChE (IC_{50} 2.57 μM), BuChE (IC_{50} 3.26 μM), and BACE-1 (IC_{50} 10.65 μM) with confirmed PAMPA-BBB permeability and self-Aβ aggregation inhibition [46]. The triazole fragment extends the planar conjugated system for enhanced fibril intercalation while providing additional H-bond acceptance analogous to the imine nitrogen of ThT. The coumarin–quinoline hybrid reported by Liu and colleagues represents an extension of this strategy in which the extended fused aromatic system provides a binding mode analogous to intercalating DNA ligands, with calculated binding affinity for the Aβ fibril inter-sheet groove of −9.9 kcal/mol [47]. Increased ring fusion, however, generally raises molecular weight towards or beyond the Lipinski boundary, reducing aqueous solubility and complicating formulation; those trade-offs must be explicitly managed in scaffold optimization and are rarely addressed in the primary literature.

Coumarin–polyphenolic acid hybrids targeting α-synuclein aggregation, which were synthesized by Wang and colleagues, demonstrated inhibition of α-synuclein inclusion formation in cellular models alongside ThT-confirmed fibril inhibition and disaggregation of pre-formed α-synuclein fibrils in vitro [48]. This study represents one of the most mechanistically comprehensive coumarin anti-aggregation investigations published to date, combining biochemical, biophysical, and cellular validation in a single framework.

Table 1 provides a consolidated critical SAR summary across substitution positions.

Table 1. The relationships between structure and activity of coumarin derivatives as anti-aggregating agents. This table represents the authors' synthesis of data from multiple primary sources; it does not represent a single study, and values should not be compared quantitatively across rows. Data on AChE are presented for research in which eEL AChE is utilized unless stated otherwise; to translate into therapeutic use, there is a need to validate human enzymes.

Position	Substitution	Biological Activity	Mechanistic Basis
C-3	Carboxamide/chalcone	Enhanced Aβ(1–42) and AChE inhibition [22,23]; disrupts α-synuclein/tau oligomers [29]	Extends conjugation; H-bond donor/acceptor engaging β-strand backbone NH; π-orbital overlap with Phe19 [22,23]
C-4	Methyl/phenyl/aryl	Moderate Aβ anti-aggregation [25]; enhanced hydrophobic contact	Occupies Val40 hydrophobic pocket within Aβ inter-sheet groove; σ–π contacts [24,25]
C-6	Long alkyl chain (C6–C8)	Dual CAS+PAS AChE inhibition [43]; anti-Aβ aggregation	Hydrophobic tail bridges CAS and PAS of AChE gorge; reinforces β-sheet groove binding [43]
C-7	–OH/–OMe/ piperazinyl/ morpholinyl	Sub-μM AChE/BuChE [37,38]; BBB permeability [42]; MAO-B inhibition [39]	π-Cation interactions with Trp279/Phe330 of AChE PAS; logP modulation controls passive BBB transport [37]
C-8	8-Hydroxy group	Most effective β-lg aggregation inhibitor [28]; neuroprotective in HT-22 cells [45]	H-bonding within hydrophobic cavity; radical scavenging via catechol-like geometry [39]
C-3+C-7 hybrid	Coumarin–quinoline/ benzotriazole	Aβ+BACE-1+AChE tri-target inhibition [47,49]	Triazole/quinoline fragments replicate ThT binding geometry within fibril channel; increased planar surface area [46]

Table 1. *Cont.*

Position	Substitution	Biological Activity	Mechanistic Basis
Ring Fusion	Pyrano-/ benzo-coumarin; chalcone–coumarin	Enhanced multi-target profile; disaggregation of pre-formed fibrils [47]	Extended π-system; improved intercalation geometry; greater van der Waals contact within fibril grooves [47]
C-3 (thio Semi carbazone)	Thiosemicarbazone at C-3 acetyl	Aβ(1–42) aggregation inhibition 80% vs. 52% for parent [30]; PAINS risk warrants orthogonal validation	Extended H-bond network; metal chelation capacity may sequester pro-aggregant Cu^{2+}/Zn^{2+} ions [30]

However, methodological variability also limits the possibility of making cross-scaffold SAR comparisons within the coumarin series. The potency values summarized in Table 1 are based on different aggregation substrates (Aβ(1–42), α-synuclein, tau, β-lg, and HEWL), different assay formats (ThT kinetics, ThT endpoint, TEM, and CD); different concentrations of coumarin used; and different stoichiometric ratios relative to the protein substrate, and as mentioned in Section 4, there are different degrees of autofluorescence control. A molecule such as, for instance, a C-3 carboxamide compound reported with an IC_{50} equal to 15 μM in one ThT assay cannot be compared with a C-7 piperazinyl compound reported with an IC_{50} equal to 8 μM in a different assay with a different substrate without adjusting these factors. Therefore, the pharmacophore map shown here should be seen as a synthesis of directional SAR trends derived from individual studies, rather than a quantitatively calibrated activity landscape valid across all reported compounds and assay systems.

Figure 4 provides a graphical SAR map summarizing favorable and unfavorable substitutions at each position of the coumarin scaffolds.

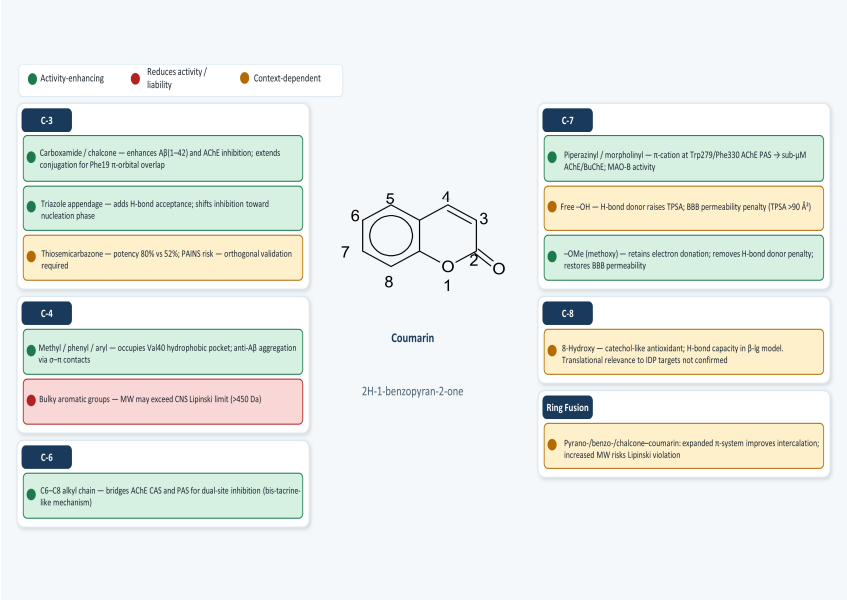

Figure 4. Graphical structure–activity relationship map of the coumarin scaffold for anti-aggregation and multi-target activity. The coumarin bicyclic core (2H-1-benzopyran-2-one) is shown at the center. Green annotations indicate substituents associated with enhanced activity in the cited literature; red annotations indicate substituents associated with reduced activity or increased physicochemical liability; amber annotations indicate substituents with context-dependent effects. All annotations reflect the directional trends summarized in Table 1 and Section 4; quantitative comparisons across substitution positions are not valid due to methodological heterogeneity of the source data. This figure is prepared by the author using Microsoft PowerPoint (Microsoft Corporation, Redmond, WA, USA).

5. Critical Appraisal of Multi-Target-Directed Ligand (MTDL) Strategies

5.1. The Pharmacological Rationale for MTDL Design in AD

The multifactorial pathogenesis of AD (including Aβ aggregation, tau hyperphosphorylation, cholinergic deficit, oxidative stress, neuroinflammation, and metal dyshomeostasis) has demonstrated the insufficiency of single-target therapeutic approaches. The clinical history is informative, in that γ-secretase inhibitors (semagacestat and avagacestat) exacerbate cognition because they prevent the Notch pathway; BACE-1 inhibitors (verubecestat, atabecestat, and lanabecestat) did not succeed in Phase III, despite success in lowering Aβ, and selective AChE inhibitors only offered temporary symptomatic relief.

The MTDL strategy is designed to produce an additive effect or potentially synergistic pharmacological effect that cannot be achieved when selective agents are administered individually, since a single molecule avoids the pharmacokinetic mismatches inherent to co-administering separate drugs. It should be noted that the term 'synergy' in this context is a pharmacological hypothesis, as the benefit of simultaneous modulation of multiple disease pathways is predicted by the MTDL framework but has not yet been shown in controlled in vivo experiments that compare the MTDL with equimolar combinations of its separate pharmacophoric systems. Although the synergy argument is very attractive for the design of MTDL, there is no direct comparative in vivo data available for the coumarin scaffold class to support this [50,51]. The coumarin backbone is geometrically and electronically efficient in the design of MTDL, as the bicyclic core is planar and therefore engages effectively with the active site of the AChE through aromatic stacking, whereas the peripheral groups project into the binding pockets of other co-targets. Its synthetic accessibility—amenable to one- or two-step derivatization by Knoevenagel condensation, Pechmann condensation, and Wittig olefination—enables rapid generation of structurally diverse focused libraries [51,52].

5.2. AChE/BuChE and Aβ Aggregation: The Canonical Coumarin MTDL Paradigm

The most extensively documented MTDL application of coumarins combines cholinesterase inhibition with anti-Aβ aggregation activity. Novel coumarin MTDLs exhibited hAChE inhibition at IC_{50} values of 28.88 and 26.03 nM—approximately ten-fold superior to donepezil—alongside hBuChE inhibition (IC_{50} 103.90 and 90.09 nM), GSK-3β inhibitory activity, and superior anti-tau and anti-Aβ aggregation relative to donepezil controls [49]. This study is notable for employing human recombinant enzyme preparations, which represent the appropriate standard for translational inference. By contrast, the majority of coumarin cholinesterase inhibitor studies reviewed here employed electric eel AChE, and the potency figures they report cannot be directly extrapolated to human enzyme inhibition because of documented differences in PAS composition between eEl AChE and hAChE, including the substitution of Asp72 (hAChE) by Glu73 (eEL AChE), which alters the electrostatic contacts governing the PAS-binding substituent affinity [37,40]. Unless a study explicitly specifies human recombinant enzymes, potency values cited in this section should be regarded as species-specific estimates not directly predictive of human enzyme inhibition.

Kinetic analysis demonstrated mixed-mode AChE inhibition, consistent with simultaneous engagement of both CAS and PAS—a mechanistic fingerprint of dual-site AChE binders that distinguishes these compounds from the competitive inhibitors that dominate the approved drug landscape.

Coumarin-based scaffolds linked to pyridinium salts via flexible aliphatic chains demonstrated nanomolar inhibition of both AChE and BuChE alongside Aβ aggregation reduction and cellular protection against H_2O_2-induced and amyloid-induced toxicity in PC12 and SH-SY5Y cells [43].

The pyridinium salt motif, though able to increase cholinesterase affinity because of cation-π interactions, raises concerns about CNS penetration due to a permanent positive charge. The original study's PAMPA-BBB data may not be sufficient to resolve this concern. PAMPA only models passive diffusion and does not take into account P-gp efflux, which must be validated in vivo before such compounds can be termed true CNS drug candidates. This is typical of a common conflict in the coumarin MTDL design: individual target affinity-optimizing substituents often cause physicochemical penalties to BBB penetration, making the resulting multi-objective optimization problem one for which few molecules satisfy all criteria simultaneously.

5.3. 3-Arylcoumarin-Triazole Hybrids: LOX, BuChE, and Neuroprotection

N-benzyl triazole-containing 3-arylcoumarins tested as 15-lipoxygenase (15-LOX) and cholinesterase inhibitors displayed BuChE and 15-LOX inhibitory effects with neuroprotective effects in H_2O_2-injured PC12 cells that surpassed quercetin and significantly lowered Aβ(1–42) aggregation. The 15-LOX target is of special interest: the metabolism of arachidonic acid through the 15-LOX pathway to hydroperoxy-eicosatetraenoic acids, which induce oxidative stress and neuroinflammation in AD brain tissue, is co-inhibited together with BuChE and Aβ aggregation inhibition; three mechanistically orthogonal pathological axes are inhibited. Critically, the absence of any anti-15-LOX activity in earlier 3-arylcoumarin series in the absence of the triazole appendage suggests the triazole nitrogen moieties play a specific role in interactions with the active sites of LOX—an SAR effect not generally seen from reviews of this compound series [52].

5.4. GSK-3β, Tau Hyperphosphorylation, and the TRKB-CREB-BDNF Axis

LM-031, a coumarin derivative, was shown to exert neuroprotective properties in neuronal cells expressing the pro-aggregated ΔK280 tau mutant, acting via the TRKB-CREB-BDNF signaling pathway and caspase activity, as well as reversing ERK hyperphosphorylation [53,54]. These findings are significant beyond the cholinergic and amyloid axes, as they demonstrate that coumarin derivatives can engage neurotrophin signaling pathways proposed as disease-modifying targets in their own right and suggest that anti-aggregation activity and neuroprotection via trophic signaling may be mechanistically dissociable. The mechanistic basis for TRKB activation by coumarin derivatives is not fully characterized; whether it reflects direct TRKB agonism, indirect effects through reduced Aβ/tau burden, or modulation of downstream kinase cascades is an important unresolved question that should guide subsequent mechanistic investigations.

5.5. Oxidative Stress, Neuroinflammation, and the Nrf2/ARE Pathway

Alkyl-substituted coumarins evaluated in the context of neurodegeneration demonstrated multi-target inhibitory profiles spanning carbonic anhydrase (CA), MAO-A/B, AChE, and BuChE, with neuroprotective activity in LPS-stimulated rat astrocytes evidenced by reduction of H_2O_2 generation and IL-6 secretion [55]. The CA inhibitory activity is mechanistically noteworthy, as CA isoforms expressed in the CNS modulate extracellular pH and inflammatory signaling, and their inhibition may contribute to the neuroprotective phenotype. Several natural coumarins, including esculetin, umbelliferone, scopoletin, and osthole, modulate the Keap1/Nrf2/ARE signaling pathway, the master transcriptional regulator of antioxidant defense [56]. Nrf2 activation induces expression of heme oxygenase-1 (HO-1), NQO1, glutamate-cysteine ligase, and thioredoxin reductase, which are enzymes that suppress ROS, maintain glutathione homeostasis, and attenuate neuroinflammation [56,57]. The neuroprotective activity of umbelliferone and imperatorin in scopolamine-induced cognitive impairment rat models, manifesting as restored spontaneous alternation behavior, reduced AChE activity, and modulation of kynurenine

pathway metabolites, provides in vivo evidence for Nrf2-mediated neuroprotection by natural coumarins that warrants extension to aggregation-prone transgenic models [58].

In vivo evidence for 3-acetyl coumarin (3-AC) demonstrated alleviation of neuroinflammatory responses and oxidative stress in an $AlCl_3$-induced AD rat model, with significant reductions in caspase-3 and NF-κβ gene expression (qRT-PCR); restoration of AChE, dopamine, and noradrenaline levels; and histopathological confirmation of normal hepatic, renal, and brain tissue architecture [17]. This study represents one of the few in vivo investigations of a synthetic coumarin derivative in an AD-relevant model, and its histopathological safety data are particularly noteworthy given hepatotoxicity concerns associated with some coumarin derivatives, as a safety dimension that deserves systematic attention in lead optimization.

6. Considerations of Pharmacokinetic Optimization and Blood–Brain Barrier Penetration

Figure 5 provides an overview of the pharmacokinetic steps a potential orally administered coumarin MTDL candidate would need to go through to achieve a therapeutically relevant free drug concentration in the brain. A traffic-light convention is used to represent the current state of evidence for published MTDL candidates: the green border represents published MTDL candidates that have been characterized at that stage; the amber border represents published MTDL candidates that have been partially characterized, but also have a critical gap; and the red border means the stage has not been characterized across the published series. As can be seen immediately in Figure 5, Stages 3 and 4 (in vivo brain exposure quantification and hepatic metabolic stability profiling) are entirely unaddressed in the literature concerning all of the coumarin MTDL candidates examined herein, except selected studies that have provided some measurement of passive permeability (Stage 2). Each step is discussed further below, with a focus on the quantitative aspects of the Stage 3 'gap', which represents the widest disconnect between in vitro results and in vivo proof-of-concept.

The failure of numerous anti-amyloid drug candidates in clinical trials has been attributed in part to insufficient CNS drug exposure, underscoring that BBB penetration is not a pharmacokinetic convenience but a fundamental efficacy requirement. Characteristics of the BBB include tight junctions between cerebral endothelial cells limiting paracellular diffusion; active efflux of the lipo-polar proteins, P-glycoprotein (P-gp/ABCB1) and breast cancer resistance protein (BCRP/ABCG2); and a lipid-rich membrane environment which supports passive transcellular diffusion of lipophilic molecules. The most commonly used physicochemical requirements of CNS drug-likeness, such as MW less than 450 Da (strong) or less than 500 Da (acceptable); logP between one and three (optimal range); a preferred TPSA of <90 $Å^2$ or <60 $Å^2$; H-bond donors < 3; H-bond acceptors < 7; and no P-gp substrate structural alerts [59,60].

The coumarin nucleus inherently satisfies all of these criteria: MW 146 Da, logP 1.39, TPSA 26.3 $Å^2$, no H-bond donors, and one H-bond acceptor. Even extensively substituted MTDL derivatives, with molecular weights in the 380–480 Da range, generally maintain TPSA values below 80 $Å^2$ and logP values in the 2–4 range [40,49,61]. Multiple studies have validated BBB penetrability using PAMPA-BBB assays: a coumarin–donepezil hybrid confirmed BBB permeability with $Pe > 4 \times 10^{-6}$ cm/s [61]; 4-trifluoromethyl-coumarin hybrids demonstrated BBB permeability [42]; and various novel coumarin derivatives were predicted to possess favorable BBB penetration by in silico tools [36].

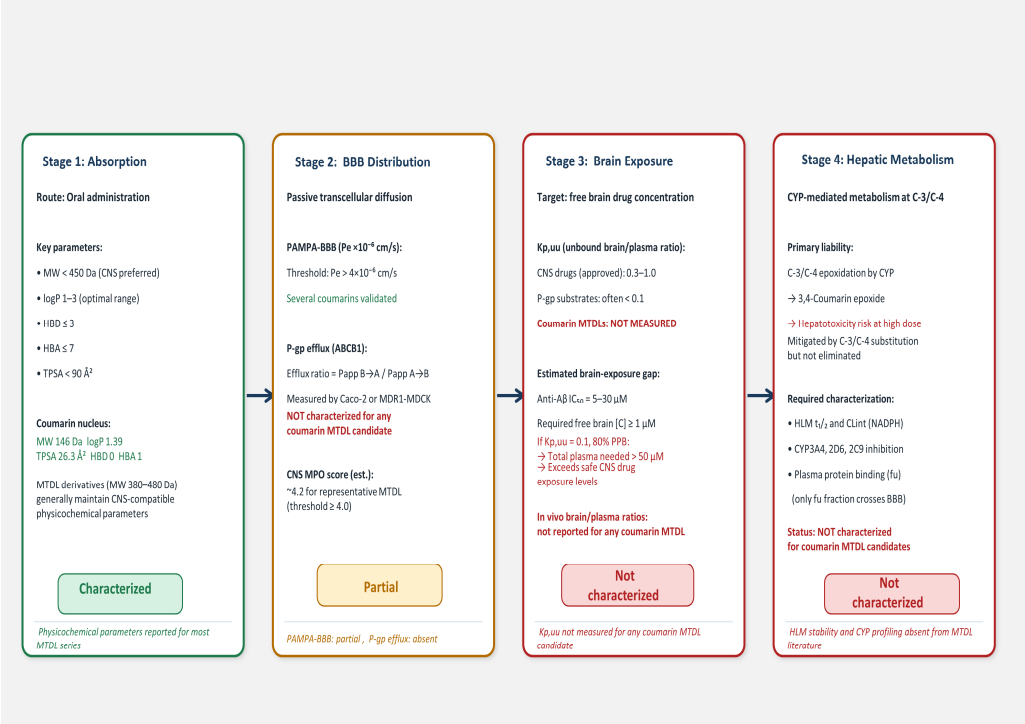

Figure 5. Pharmacokinetics and drug delivery aspects of coumarin MTDL candidates delivered to the CNS. The figure has a schematic pipeline design with four successive stages. Stage 1 (Absorption): orally administered, relevant parameters: MW, LogP, and HBD count based on CNS drug-likeness. Stage 2 (Distribution): blood compartment-plasma protein binding equilibrium (fu, plasma); passive transcellular BBB diffusion as a gradient arrow; and competitive efflux vector: P-gp on the luminal side of the BBB. Stage 3 (Brain exposure): brain parenchyma with free drug concentration (Kp,uu × fu, plasma × cplasma); target engagement threshold is represented by a dashed horizontal line, at 1 µM (lower bound of anti-Aβ IC_{50} in best-performing coumarins). Stage 4 (Metabolism): hepatic CYP-mediated epoxidation at C-3/C-4 shown as a structural arrow; 3,4-coumarin epoxide metabolite indicated with hepatotoxicity risk notation. Color coding: red = stages that are not characterized in the literature for any of the coumarin MTDLs; green = stages that are well characterized for at least one coumarin MTDL in published literature. The graph shows that there are no P-gp efflux characterization data or plasma protein binding data, nor a determination of in vivo brain/plasma ratio data for any of the coumarin MTDL candidates reviewed. This is a schematic drawing prepared by the authors using Microsoft PowerPoint (Microsoft Corporation, Redmond, WA, USA).

Critical evaluation of these data, however, reveals a systematic methodological shortcoming: PAMPA-BBB assays model passive transcellular diffusion only and do not account for P-gp-mediated efflux, which has been responsible for the clinical failure of numerous CNS drug candidates despite adequate passive permeability [59,60]. None of the published coumarin MTDL studies have characterized P-gp substrate affinity using Caco-2 bidirectional transport assays or MDR1-MDCK cell systems. This represents a gap that cannot be addressed retroactively once in vivo studies are initiated. The predictive accuracy of in silico BBB tools such as SwissADME, benchmarked at approximately 72–78% classification accuracy for CNS-positive versus CNS-negative compounds, means that approximately one in four compounds predicted as BBB permeable will fail experimental validation [62]. Machine learning-based models trained on larger, more structurally diverse datasets—LightBBB, Deep-B3, and BBBpred—demonstrate improved performance but are not uniformly employed in the coumarin anti-aggregation literature [63].

The available physicochemical and in vitro permeability data can be used to derive a quantitative estimate of the brain-exposure gap. A representative optimized coumarin MTDL with MW ~420 D, logP 2.8, TPSA 72 $Å^2$, and PAMPA-BBB Pe ~5 × 10^{-6} cm/s has

an estimated CNS multiparameter optimization (MPO) score of ~4.2 on the Wager scale, which is within the "acceptable" CNS range of ≥ 4.0 [64]. However, the permeability of PAMPA is not correlated with the in vivo permeability of the brain (Kp,uu) and is also complicated by P-gp efflux. Median unbound brain-to-plasma ratios (Kp,uu) are around 0.3–1.0 for drugs that have been approved as CNS drugs at the time of writing and are typically < 0.1 for P-gp substrates in rodents [65]. The plasma-free drug concentration of at least 10 μM would be necessary if Kp,uu = 0.1, which is a conservative lower limit because anti-Aβ aggregation IC_{50} values for the most effective coumarins used were reported to be 5–30 μM for plasma, corresponding to 80% plasma protein binding of the compounds. Such an exposure dose is significantly higher than that which could be obtained at approved, well-tolerated dosage levels of CNS drugs, and no coumarin MTDL has been characterized in a pharmacokinetic study that would allow a quantitative comparison [65]. Although this analysis is necessarily approximate, in the absence of in vivo coumarin pharmacokinetic data, it appears that the brain-exposure gap is not just a translation-related inconvenience but rather a quantitative pharmacological barrier for any kind of coumarin derivative to be considered a possible CNS drug candidate.

The introduction of fluorine atoms into coumarin derivatives simultaneously addresses multiple pharmacokinetic objectives: metabolic stabilization through blockade of CYP-mediated aromatic hydroxylation at C-3 and C-4; enhanced lipophilicity (F logP increment ≈ +0.14–0.25 per fluorine); improved membrane permeability; and, in the specific case of CF_3, creation of strong electron-withdrawing effects that improve binding to aspartyl protease active sites such as BACE-1 [61]. These multiple beneficial effects of fluorination are well-appreciated in CNS medicinal chemistry generally but have been deployed in only a small subset of the coumarin anti-aggregation literature, suggesting substantial scope for fluorine bioisosterism as a pharmacokinetic optimization strategy.

Table 2 provides a minimum pharmacokinetic characterization panel recommended for any coumarin anti-aggregation lead before in vivo efficacy studies are initiated.

Table 2. Minimum pharmacokinetic assays recommended for coumarin anti-aggregation lead compounds before in vivo efficacy studies. This table represents the authors' data collection from established CNS drug development guidelines and reported coumarin PK data.

Assay	Parameter Measured	Method	Reference Standard
PAMPA-BBB	Passive transcellular permeability (Pe, $\times 10^{-6}$ cm/s)	Porcine brain lipid in dodecane, 16 h, 25 °C [66,67]	Donepezil (CNS+ control)
Caco-2 bidirectional transport	Efflux ratio (Papp B→A/ Papp A→B)	21-day differentiated Caco-2 monolayer, pH 7.4, 2 h [68,69]	Digoxin (P-gp substrate control)
Plasma protein binding	% Bound	Equilibrium dialysis (human plasma) [70]	Warfarin (high binding)
Microsomal stability	$t_{1/2}$ (min), CLint (μL/min/mg)	Human liver microsomes, NADPH-supplemented [71]	Verapamil (low stability control)
CYP inhibition	IC_{50} (μM) against CYP3A4, 2D6, 2C9	Human liver microsomes, NADPH-supplemented [72,73]	Ketoconazole (CYP3A4 inhibitor control)

In addition to BBB penetration, systematic characterization of metabolic stability, protein binding, and toxicological liability are necessary for the translational advancement of coumarin MTDL candidates. For the coumarin class, a particular concern is microsomal instability (by CYP-mediated epoxidation), where an epoxide forms at the C3-C4 double bond of the parent coumarin, and the resulting 3,4-coumarin epoxide has been associated with hepatotoxicity; this can be reduced but not prevented by C-3 and C-4 substitution [74]. Therefore, for all leads, a human liver microsomal stability assay should be included in the lead panel along with CYP inhibition assays of the most relevant isoforms that can cause CNS drug interactions, namely CYP3A4, CYP2D6, and CYP2C9. Another factor affecting CNS exposure is plasma protein binding: only unbound (fu, plasma) is available to cross the BBB, and compounds with high protein binding (>99%, fu, plasma <0.01) will have very low effective CNS concentrations relative to the total plasma concentrations [75]. Equilibrium dialysis against human plasma should be included in the minimum characterization panel.

Also, the prodrug strategies represent a mechanistically rational approach for enhancing the translational pharmacology of coumarin MTDLs: esterification of the C-7 hydroxyl group to increase membrane permeability in the form of acyl esters that are metabolized to the phenols in the CNS to increase the amount of drug available for target binding, or conjugation with GLUT1 or LAT1 substrate vectors to enhance active CNS transport, could substantially improve both BBB penetration and metabolic stability without compromising target affinity [76].

Table 3 provides a comparison of the best-characterized coumarin MTDL candidates against the approved cholinesterase inhibitors donepezil and galantamine across the relevant parameters for translational advancement. Where human enzyme data are available, they are indicated; eEL AChE data are labeled accordingly. This comparison shows that while certain coumarin derivatives approach or match approved drugs on individual target affinity metrics, none has been characterized across the full parameter set required for meaningful translational benchmarking. Also, measured brain/plasma ratios and in vivo efficacy in amyloid-overexpressing transgenic models are absent for all coumarin candidates.

Table 3. Comparative profile of representative coumarin MTDLs. Candidates versus approved cholinesterase inhibitors on key translational parameters. This table represents the authors' synthesis of data drawn from multiple primary sources.

Compound	AChE IC_{50} (Nm)	Enzyme Source	Anti-Aβ IC_{50}	PAMPA-BBB Pe	Brain/Plasma Ratio (In Vivo)	Transgenic Model Efficacy
Donepezil [77]	6.7	hAChE	Not a primary mechanism	$>4 \times 10^{-6}$ cm/s	~1.0 (Kp,uu)	Yes
Galantamine [78]	800	hAChE	Not a primary mechanism	High (passive)	~0.8	Yes
Abd El-Mageed et al. [49]	28.88	hAChE	NR (ThT, unvalidated)	Not Measured	Not measured	None
Liu et al. [35]	1313	eEL AChE	NR	$Pe > 4 \times 10^{-6}$ cm/s	Not measured	None
Wang et al. [48]	NR	-	10–30 μM (ThT+TEM)	Not Measured	Not measured	None
3-AC (Zeb et al.) [17]	Reduced In vivo	Rat brain	Reduced in vivo	Not Measured	Inferred, not measured	$ALCL_3$ rat (non-transgenic)

NR: not reported, eEL: electric eel, hAChE: human recombinant AChE.

7. Applications Across Disease-Relevant Amyloidogenic Targets

Figure 6 provides a comparative overview of the three disease-specific amyloid targets addressed in this review (Aβ(1–42) in AD, α-synuclein in PD, and IAPP in T2DM); the data have been arranged to ensure that the differences in depth of evidence are instantly apparent. The left panel summarizes the strongest evidence, namely that the structure of Aβ(1–42) fibrils can be resolved to near-atomic resolution using cryo-EM across various polymorphs; the Phe19–Val40 inter-sheet groove contains a structurally defined site for coumarin binding; and a series of computational and biophysical studies concur on the existence of a conventional coumarin-binding site in the inter-sheet groove but fail to provide proper structural confirmation. The center panel reflects an intermediate state of evidence because α-synuclein is intrinsically disordered and lacks a defined inter-sheet groove for binding site assignment; docking scores against the NAC region are modest relative to Aβ (−4.5 versus −7.5 to −9.9 kcal/mol). Even though coumarin–polyphenolic hybrids exhibit biophysical and cellular anti-aggregation activity, no structural data for coumarin–α-synuclein fibrils are available. The right panel identifies the most significant gap in the literature despite a structurally compelling rationale: IAPP FGAILS is a π-stacking aggregation driver that is found at Phe23, which is structurally equivalent to Phe19 in Aβ(1–42), and near-atomic cryo-EM structures of IAPP fibrils exist, but none of the coumarin derivatives have been investigated as inhibitors of IAPP aggregation. Each target is discussed in turn in the three subsections below, using Figure 6 throughout to set a context for each target.

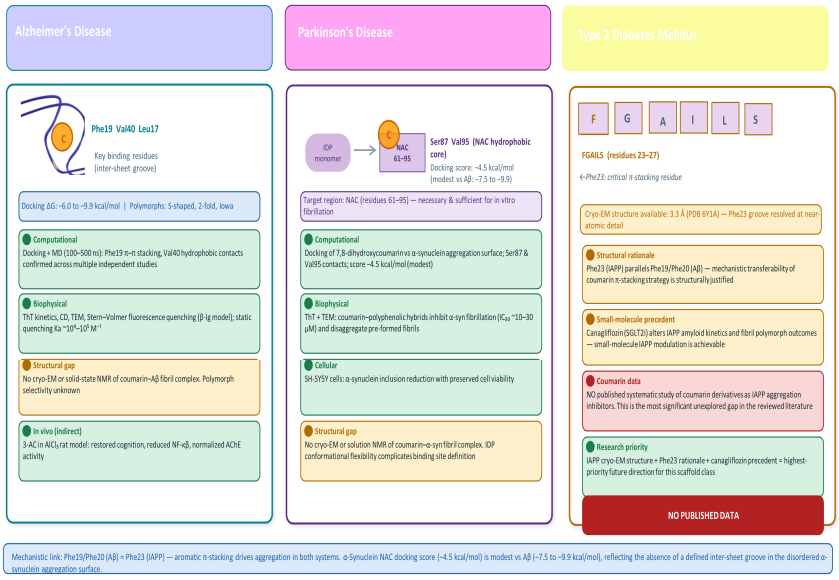

Figure 6. The design considerations of coumarin inhibitors and amyloid targets to treat various diseases. A schematic side-by-side showing three disease contexts. The left panel (AD) shows an inter-sheet groove (Phe19 to Val40) within the S-shaped cross-section of the Aβ(1–42) fibril (cryo-EM-derived, schematic), the tau PHF is shown separately, and the binding mode of coumarin is indicated. Unstructured α-synuclein NAC (residues 61–95) in the center panel (PD); hydrophobic NAC residues (NC) shown interacting with the docked molecule; docking score range (−4.5 kcal/mol) indicated in parentheses; and strength of docking interaction labelled as modest when compared to docking interactions for Aβ. Highlighted in the right panel (T2DM): IAPP fibril with FGAILS segment (residues 23–27), structural representation of the candidate with no published data and a research priority arrow for the coumarin. The figure conveys the concept of asymmetry in the level of evidence for various disease targets. This is an original schematic drawing by the author using Microsoft PowerPoint (Microsoft Corporation, Redmond, WA, USA).

7.1. Alzheimer's Disease: Aβ Aggregation, Tau, and Cellular Neuroprotection

Cellular evidence for coumarin anti-aggregation activity in AD-relevant models is mounting but requires critical contextualization. Compounds ZN014 and ZN015 reduced Aβ aggregation, caspase-1 activity, oxidative stress, and AChE activity while increasing neurite outgrowth and BDNF/TRKB pathway activation in SH-SY5Y cells expressing a GFP-tagged Aβ folding reporter [4,22,38]. These multi-modal neuroprotective effects at low micromolar concentrations in a human neuroblastoma line are encouraging; however, the GFP-Aβ reporter system detects changes in Aβ folding kinetics rather than true fibril formation, and neuroblastoma cells differ from primary neurons in aggregation kinetics, membrane composition, and stress response pathways. Direct extension to primary neuron cultures or in vivo transgenic models has not been reported.

For tau inhibition, LM-031 and related chalcone–coumarin hybrids inhibited misfolding of ΔK280 tau and tau P301L aggregation in 293T cell models [53,54,79]. In ΔK280 tau_RD-expressing neuronal cells, coumarin derivatives reduced aggregate burden assessed by thioflavin S staining, decreased caspase-3 activity, and restored BDNF signaling through TRKB phosphorylation and CREB activation [53,54]. The ΔK280 mutation dramatically accelerates tau aggregation and is directly relevant to FTLD-tau pathology, though it may not fully recapitulate the aggregation kinetics of sporadic AD tau. The observation that quercetagitrin, which is a quercetin glycoside structurally related to coumarin polyphenols, blocked tau accumulation and reversed cognitive deficits in P301S-tau transgenic mice following oral administration provides in vivo proof-of-concept for translatability that must now be pursued for optimized coumarin compounds [40].

The most comprehensive in vivo evidence for coumarin neuroprotection in an AD-relevant context comes from the 3-AC study, demonstrating restoration of cognitive behavior (Y-maze spontaneous alternation), reduction of NF-κβ-driven neuroinflammation, and normalization of monoaminergic neurotransmitters in $AlCl_3$-treated rats [17]. $AlCl_3$-induced neurodegeneration recapitulates several AD-relevant pathological features, including oxidative stress, cholinergic deficit, and tau phosphorylation, but does not produce amyloid plaques. In vivo evidence in genetically defined amyloid-overexpressing transgenic models—5XFAD, APP/PS1, or 3xTg-AD—remains the critical unmet benchmark for this scaffold class [80].

7.2. Parkinson's Disease: α-Synuclein Aggregation and Coumarin-Polyphenolic Hybrids

α-Synuclein, an intrinsically disordered 140-residue protein, undergoes pathological misfolding into a β-sheet-rich structure in PD. The aggregation-prone NAC region (residues 61–95) is both necessary and sufficient for in vitro fibrillation and is enriched in hydrophobic, β-sheet-promoting residues [81–83]. Small-molecule inhibitors must engage the NAC region either directly or by stabilizing non-fibrillar conformations, presenting a mechanistic challenge distinct from the more structurally defined Aβ fibril groove.

Coumarin–polyphenolic acid hybrids designed by Wang and colleagues demonstrated multi-stage inhibitory activity against α-synuclein: ThT fluorescence assays confirmed fibril inhibition (IC_{50} ~10–30 μM for the most active compounds); TEM confirmed disaggregation of pre-formed α-synuclein fibrils; and cellular assays in SH-SY5Y cells demonstrated reduction of α-synuclein inclusion formation with concurrent preservation of cell viability [48]. The molecular design principle, conjugating caffeic or ferulic acid fragments to the coumarin nucleus through amide bonds, is pharmacologically well-reasoned, since polyphenolic acids have independently established α-synuclein binding activity through aromatic interactions with hydrophobic NAC residues. In silico docking of 7,8-dihydroxycoumarin against the α-synuclein aggregation surface identified Ser87 and Val95 as key interacting residues within the NAC domain, with a docking score of −4.5 kcal/mol, which is consid-

ered modest compared to values reported for Aβ fibril binding (−7.5 to −9.9 kcal/mol) but establishes the geometric feasibility of coumarin intercalation into the α-synuclein aggregation surface [13,84]. Cryo-EM or solution NMR structural characterization of coumarin binding to α-synuclein fibrils or oligomers remains an outstanding methodological priority.

7.3. Type 2 Diabetes Mellitus: IAPP as an Underexplored Target with Significant Therapeutic Opportunity

Islet amyloid polypeptide (IAPP), also known as amylin, is a 37-residue peptide co-secreted with insulin whose pathological aggregation, driven by the FGAILS sequence (residues 23–27) containing the critical Phe23 aromatic residue, leads to amyloid deposition in pancreatic islets of over 70% of T2DM patients at autopsy and is causally associated with progressive β-cell loss [85,86]. The IAPP system is pharmacologically significant for reasons that extend well beyond its isolated disease relevance. First, it constitutes a distinct amyloid target for which no approved anti-aggregation therapeutics exist. Second, it shares structural amyloidogenicity determinants, particularly aromatic π-stacking at Phe23 with Aβ at Phe19/Phe20, suggesting mechanistic transferability of coumarin intercalation strategies. Third, the co-deposition of IAPP and Aβ in both pancreatic and AD brain tissue, alongside epidemiological evidence that T2DM patients carry a 1.5–2.5-fold elevated AD risk, has prompted credible hypotheses of IAPP–Aβ cross-seeding that implicate IAPP aggregation directly in neurodegeneration [25,85,87].

Despite these compelling reasons for investigation, the published literature contains essentially no systematic study of coumarin derivatives as IAPP aggregation inhibitors. This absence of data is a notable gap in the coumarin anti-aggregation literature, particularly given the structural rationale, available cryo-EM structural data, and precedent for small-molecule IAPP modulation described below. This lack of data is not explained by technical limitations, as IAPP aggregation can be easily measured by ThT fluorescence using existing protocols, and the structure of IAPP fibrils has been resolved by cryo-EM at near-atomic resolution; Cao et al. reported a 3.3 Å resolution cryo-EM structure of human IAPP fibrils that provides atomic-level detail of the Phe23-containing FGAILS aggregation core [88], making structure-guided inhibitor design directly feasible for this target. The recent finding that the licensed SGLT2 inhibitor canagliflozin can restructure the kinetics of IAPP amyloid formation and modify the outcome of fibril polymorph directly demonstrates that IAPP aggregation can be therapeutically modulated using small molecules, confirming that the structural understanding needed to guide such modulation is already in hand [89]. Coumarins structurally optimized for Aβ inhibition represent a candidate for systematic evaluation against IAPP, and this research should be prioritized.

7.4. Mechanistic Insights and Translational Limitations of Model Protein Systems

Hen egg white lysozyme (HEWL) and β-Lactoglobulin (β-lg) have been the native exemplary model protein systems used to elucidate coumarin anti-aggregation action mechanistically. Multi-spectroscopic characterization in β-lg systems established that coumarin binding occurs at the hydrophobic binding site of native β-lg, with thermodynamic parameters derived from Van 't Hoff analysis indicating predominantly enthalpic, H-bond-driven binding ($\Delta H < 0$, $\Delta S < 0$) [25,26,28]. HEWL aggregation inhibition and disaggregation by 4-methyl and 4-methylthiocoumarin were confirmed by TEM and CD, with the 4-methylthio compound demonstrating superior disaggregation activity attributed to the additional hydrophobic contribution of the sulfur-containing substituent [26].

These model systems provide mechanistic insights but must be interpreted with substantial translational caution. β-lg and HEWL are globular, ordered proteins with defined hydrophobic binding sites that are absent in IDPs such as Aβ, α-synuclein, and tau. The binding mode of coumarins to β-lg through stabilization of a native hydrophobic

site is mechanistically distinct from intercalation into the cross-β fibril groove proposed for Aβ inhibition. Thermodynamic parameters derived from native protein binding cannot be extrapolated to disordered monomers or nucleating oligomers of amyloidogenic IDPs. Future mechanistic studies should prioritize truncated amyloidogenic peptide systems ($A\beta_{16–22}$, $IAPP_{22–29}$) for which cryo-EM fibril structures are available and ligand binding can be characterized by solution NMR—approaches that would directly bridge the gap between model system data and therapeutic hypotheses.

8. Computational Methods: Mechanistic Insights, Limitations, and Emerging Approaches

Computational methodologies have played an indispensable role in elucidating coumarin binding modes and rationalizing SAR data. Molecular docking employing AutoDock Vina, GLIDE, or GOLD against Aβ fibril structures (PDB IDs: 2BEG, 5KK3, and 7Q4B) has characterized binding at the Phe19–Val40 inter-sheet groove, reporting free energies of −6.0 to −9.9 kcal/mol for optimized coumarins, with extended conjugated systems and strategic C-3 and C-7 substitutions consistently associated with the highest affinities [22,23,25,90].

Molecular dynamics simulations extending up to 100–500 ns have incorporated protein flexibility and explicit solvent effects. Coumarin molecules using 100 ns MD increased C-alpha–C-alpha distances between Phe19 and Val40 by approximately 0.8 Å and reduced the mean β-strand count per oligomer in Aβ simulations, consistent with physical disruption of inter-sheet contacts [22]. Quantum mechanical support for the intercalation hypothesis has been provided by DFT calculations at MP2 and B3LYP levels, which quantify π-stacking interaction energies and charge distributions [9,23,91].

In silico ADMET prediction tools like SwissADME, pkCSM, ADMETlab 2.0, and ProTox-3.0 are now regularly reported alongside biological activity data in published coumarin research projects [36,49]. The BBB prediction model of SwissADME is predictive on a variety of CNS drug datasets, and indicates that about a quarter of the compounds that are predicted to be BBB-positive will not pass in vitro or in vivo BBB assays [62]. These tools must be interpreted as initial filtering aids, not as definitive pharmacokinetic forecasts. Their popularity in the literature and lack of in vitro BBB validation are systematic flaws in the coumarin anti-aggregation literature that need to be tackled by the entire field. Docking scores also have poor correlation with experimentally measured binding affinities, especially when using flexible or polymorphic targets like amyloid fibrils. The surface flexibility of the A2 fibril cannot be well modeled by protocols of static docking, and the structural polymorphism issue in Section 3.2 implies that docking to only one polymorph structure gives us a biased understanding of the binding in the real world.

The recent development of the cryo-EM structure solution of small-molecule complexes with amyloid fibrils at a near-atomic resolution provides revolutionary opportunities in structure-guided coumarin design. Fragment-based drug discovery (FBDD) workflows on these cryo-EM structures could discover minimal coumarin-derived binding fragments whose expansion by computational growing and merging algorithms gives experimentally optimized leads with validated binding modes.

Generative AI molecular design tools and structure-prediction models such as AlphaFold2 have demonstrated utility in predicting conformational ensembles of folded proteins; however, their application to amyloid-forming intrinsically disordered proteins (IDPs) remains limited and technically challenging, as the conformational landscape of IDPs differs fundamentally from that of folded proteins. Current IDP-specific modeling approaches are in early stages of development and require rigorous experimental validation before mechanistic conclusions can be drawn.

9. Discussion

The evidence reviewed in this paper provides convergent computational and indirect biophysical support for a mechanistically consistent model in which the coumarin scaffold interacts with amyloid β-sheet structures through an intercalative mechanism. This model is supported by molecular docking, MD simulation, DFT energy calculations, and indirect biophysical measurements but has not yet been confirmed by direct structural methods such as cryo-EM co-crystal structures or solution NMR of coumarin fibril complexes.

The convergent computational, biophysical, and biochemical evidence of this mechanistic model is supported by numerous independent research studies. However, there are several underlying tensions within the literature that require sensitive consideration.

Tension 1: In Vitro Potency vs. Translational Relevance.

The anti-Aβ aggregation of coumarin derivatives has IC_{50} values of 10–100 μM, which are better than those of the same compounds against AChE (nM-μM) or BACE-1 (μM). Such a potency difference is an intrinsic thermodynamic difficulty of suppressing a nucleation-dependent self-assembly process, which needs stoichiometrically significant concentrations of inhibitor to change the monomer-fibril equilibrium. Its clinical implication is substantial, such that systemic exposures would be necessary to get 10–100 μM free drug concentrations in the brain parenchyma, which would not be consistent with acceptable safety margins. This consideration has not been directly discussed in published coumarin SAR studies, which only report the IC_{50} values, without situating them within this pharmacokinetic context, a gap that future publications should address.

Tension 2: Methodological Heterogeneity and the ThT Fluorescence Problem.

ThT fluorescence is the primary or sole anti-aggregation endpoint in the vast majority of reports reviewed here. It is a sensitive and convenient high-throughput assay, but its limitations are well-established: ThT binds non-selectively to all kinds of β-sheet structures, not exclusively amyloid fibrils; autofluorescence of test compounds (including several fluorescent coumarin derivatives) can produce false-positive or false-negative results [33]; fluorescence is affected by pH, ion concentrations, and inner filter effects from colored compounds; and appropriate controls are essential for reliable interpretation [33,34]. Very few published coumarin anti-aggregation studies employ orthogonal validation (TEM, atomic force microscopy, dynamic light scattering, or native PAGE for oligomers) alongside ThT. This systematic deficiency may reflect assay artifacts rather than genuine inhibitory activity. Future publications in this area should require, as a minimum, TEM or CD alongside ThT for any coumarin derivative whose fluorescence spectrum overlaps with the ThT emission window.

Tension 3: Fibril Structural Polymorphism.

Cryo-EM studies have demonstrated that Aβ(1–42) fibrils adopt at least four distinct polymorphic structural variants with different inter-sheet groove geometries [4]. Docking and MD studies of coumarins have, without exception, employed a single fibril polymorph structure. Whether the anti-aggregation activity observed in ThT assays (where multiple polymorphs form simultaneously) is driven by interactions with all polymorphs or preferentially with one is entirely unknown for any coumarin derivative. If coumarin binding is highly polymorph-selective, then efficacy will depend on which polymorphs predominate in any given biological or patient-derived sample, creating fundamental uncertainty about translational relevance.

Tension 4: Non-Human Enzyme Systems for Cholinesterase Assays.

As detailed in Section 4.3, the majority of published coumarin AChE inhibition data were generated using eEL AChE rather than human recombinant hAChE. Given the substantial differences in PAS composition between species, potency data from non-human enzyme systems may not accurately predict human activity [37,40]. This limitation is

rarely acknowledged in the primary literature and represents a systematic concern for the translatability of MTDL candidates.

Nevertheless, in spite of these serious limitations, the field has achieved substantive mechanistic advances. The identification of a conserved π-stacking binding mode across structurally diverse coumarin derivatives, the demonstration of simultaneous multi-target inhibition with nanomolar AChE activity for selected compounds evaluated against human recombinant enzyme, the in vivo neuroprotective findings in the $AlCl_3$ in rat models [17], and the development of coumarin-polyphenolic acid hybrids displaying both α-synuclein inhibitory and disaggregation activity [48] collectively represent meaningful progress toward a pharmacologically credible scaffold class.

The mechanistic integrity of the intercalation model, its compliance with established aromatic chemistry and supramolecular recognition principles, and structural similarities to clinically approved amyloid-binding dyes give the intercalation model a scientifically viable base to further develop the scaffold class [9,14,23].

10. Conclusions

The mechanistic, structural, and pharmacological literature on coumarins as inhibitors of pathological protein aggregation has been critically reviewed, with emphasis on the evidence supporting the proposed β-sheet intercalation model and the pharmacological obstacles that lie between in vitro evidence and clinical relevance. Six principal conclusions are drawn.

The coumarin pharmacophore represents a geometrically well-defined and mechanistically consistent platform of amyloid β-sheet intercalation via π–π stacking at Phe19, hydrophobic contact at Val40, and complementary hydrogen bonding at the C-2 carbonyl, which shows a multivalent binding mode with convergent computational, biophysical, and biochemical proof.

Systematic SAR exploration across C-3 to C-8 has produced compounds with nanomolar AChE potency and micromolar anti-aggregation activity, with the C-7 position appearing to be the main determinant of cholinesterase selectivity and BBB permeability and C-3 as the main location of anti-aggregation elaboration.

The coumarin pharmacophore has been found in MTDL strategies showing the capability to simultaneously inhibit AChE, BuChE, GSK-3β, BACE-1, MAO-B, and amyloid aggregation, with cellular neuroprotection validated in human neuroblastoma and PC12 cell models. Nanomolar AChE inhibitory activity has been demonstrated for select derivatives using human recombinant hAChE [49]; however, the majority of published cholinesterase data were generated using electric eel AChE and cannot be directly extrapolated to human therapeutic predictions without revalidation in human enzyme systems.

The translational gap between in vitro IC_{50} values (10–100 μM to inhibit aggregation) and attainable brain concentrations remains the field's defining pharmacological challenge, and it is not adequately addressed in existing research.

Systematic uncertainties in comparative assessment of compound activity that are associated with critical methodological limitations include the use of ThT as the only anti-aggregation endpoint, lack of P-gp efflux characterization, and use of non-human enzyme preparations that need to be addressed in future studies.

The application of coumarins to IAPP inhibition in T2DM, which is supported by recently solved cryo-EM structures of IAPP fibrils and the precedent of small-molecule IAPP modulators, remains essentially unexplored, constituting a high-priority future direction that the field should pursue urgently.

11. Future Directions

11.1. In Vivo Validation in Genetically Defined Transgenic Models

The highest priority is strict in vivo testing of top coumarin MTDL hits in genetically characterized transgenic mouse models of AD (5XFAD, APP/PS1, and 3xTg-AD), PD (A53T-α-syn, and SNCA-overexpressing models), and IAPP-transgenic T2DM models. Required study elements include dose–response pharmacokinetic characterization with measured brain/plasma ratios and free brain drug concentrations; cognitive behavioral endpoints (Morris water maze, novel object recognition, and contextual fear conditioning); histopathological quantification of amyloid burden; target engagement biomarkers (AChE activity in brain, CSF Aβ42/40, and pTau181/217 where applicable); and systematic safety assessment including hepatotoxicity screening. Without such data, no coumarin derivative can be advanced beyond in vitro lead status.

11.2. Systematic Selectivity Profiling Across Amyloid Substrate

Systematic comparative SAR studies employing identical coumarin compound libraries against Aβ, tau, α-synuclein, and IAPP aggregation in parallel, using standardized assay conditions with orthogonal validation (ThT plus TEM or CD), are essential to delineate the structural determinants of target selectivity. Such studies would establish whether selectivity is achievable through rational design or whether the coumarin pharmacophore constitutes a pan-amyloid scaffold. Either conclusion carries therapeutic value: selective inhibitors would be optimized for disease-specific indications; pan-amyloid inhibitors would be candidates for diseases with co-occurring amyloid pathologies.

11.3. Cryo-EM Guided Fragment-Based Drug Discovery and Covalent Probe Development

FBDD applied to cryo-EM fibril structures—now feasible at below 2.5 Å resolution for multiple amyloid fibril types—represents the most scientifically rigorous approach to coumarin optimization. The compact coumarin bicyclic system is an ideal fragment for growing campaigns guided by cryo-EM difference density maps of fragment–fibril complexes. Covalent probe strategies, utilizing mild electrophilic warheads (acrylamide, vinylsulfone, cyanoacrylate) appended to coumarin scaffolds to engage nucleophilic Cys or Lys residues proximal to the inter-sheet groove, would provide irreversible fibril-binding tools for mechanistic studies and constitute a structurally distinct class of anti-aggregation agents.

11.4. P-gp Efflux Characterization and Prodrug Strategies

All compounds reaching lead status must be characterized for P-gp substrate affinity using Caco-2 bidirectional transport assays before in vivo studies are initiated. Compounds identified as P-gp substrates should be evaluated for structural modification (elimination of basic nitrogen, reduction of H-bond donor count, and MW reduction) or encapsulation in nanoparticle delivery systems that overcome efflux. Brain-targeted prodrug strategies, such as conjugation of coumarin MTDLs to GLUT1 or LAT1 targeting vectors, represent an underexplored approach to circumventing BBB efflux for this scaffold class.

11.5. AI-Assisted Scaffold Exploration and Priority IAPP-Targeted Design

Generative AI molecular design models, including graph neural network generators (REINVENT and GraphINVENT), diffusion-based models (DiffSBDD), and large language model-based chemical generation, trained on coumarin-specific pharmacophoric constraints and validated amyloid fibril structural data from cryo-EM databases, offer the potential to access novel coumarin derivatives with substantially improved potency,

selectivity, and pharmacokinetic profiles beyond what is accessible through conventional analogue synthesis.

Simultaneously, IAPP-focused coumarin design represents a high-priority, essentially unexplored area for medicinal chemistry. The cryo-EM structures of IAPP fibrils (PDB 9GZS, resolved to 3.4–4.0 Å) provide atomic-level detail of the Phe23-containing aggregation hotspot. The demonstration that canagliflozin alters IAPP amyloid kinetics and fibril polymorph outcomes provides direct evidence that small-molecule IAPP modulation is achievable. Coumarins structurally optimized for the FGAILS amyloidogenic region of IAPP, guided by these cryo-EM structures and validated in human islet cell models and transgenic IAPP-overexpressing rodent models, represent perhaps the most impactful translational opportunity available to this field in the near term.

Funding: This research received no external funding.

Data Availability Statement: No new data were created or analyzed in this study.

Acknowledgments: The author thanks BioRender for the figure and Graphical Abstract, which were produced from https://BioRender.com. The author used AI-assisted language editing tools (QuillBot Paraphrasing Tool) solely to improve the clarity and grammar of the manuscript. The author reviewed and edited the output and take full responsibility for the content of the publication.

Conflicts of Interest: The author declares no conflict of interest.

Abbreviations

The following abbreviations are used in this manuscript:

Aβ	Amyloid-β peptide
AD	Alzheimer's disease
AChE	Acetylcholinesterase
ADMET	Absorption, distribution, metabolism, excretion, and toxicity
APP	Amyloid precursor protein
ARIA	Amyloid-related imaging abnormalities
BACE-1	β-site amyloid precursor protein cleaving enzyme 1
BBB	Blood–brain barrier
β-lg	β-Lactoglobulin
BCRP	Breast cancer resistance protein
BuChE	Butyrylcholinesterase
CA	Carbonic anhydrase
CAS	Catalytic anionic site
CD	Circular dichroism
CNS	Central nervous system
DFT	Density functional theory
EGCG	Epigallocatechin-3-gallate
FBDD	Fragment-based drug discovery
FDA	U.S. Food and Drug Administration
GSK-3β	Glycogen synthase kinase-3β
HEWL	Hen egg-white lysozyme
HO-1	Heme oxygenase-1
IDP	Intrinsically disordered protein
IAPP	Islet amyloid polypeptide (amylin)
IC_{50}	Half-maximal inhibitory concentration
logP	Partition coefficient
MAO-B	Monoamine oxidase B
MD	Molecular dynamics
MTDL	Multi-target-directed ligand

MW	Molecular weight
NAC	Non-amyloid component
NFT	Neurofibrillary tangle
NMR	Nuclear magnetic resonance
Nrf2	Nuclear factor erythroid 2-related factor 2
PAMPA-BBB	Parallel artificial membrane permeability assay for BBB
PAINS	Pan-assay interference compounds
PAS	Peripheral anionic site
PD	Parkinson's disease
PHF	Paired helical filament
PICUP	Photoinduced cross-linking of unmodified proteins
P-gp	P-glycoprotein
ROS	Reactive oxygen species
SAR	Structure–activity relationship
ssNMR	Solid-state NMR
T2DM	Type 2 diabetes mellitus
TEM	Transmission electron microscopy
ThT	Thioflavin T
TPSA	Topological polar surface area
TRKB	Tropomyosin receptor kinase B

References

1. Dorsey, E.R.; Elbaz, A.; Nichols, E.; Abbasi, N.; Abd-Allah, F.; Abdelalim, A.; Adsuar, J.C.; Ansha, M.G.; Brayne, C.; Choi, J.-Y.J.; et al. Global, Regional, and National Burden of Parkinson's Disease, 1990–2016: A Systematic Analysis for the Global Burden of Disease Study 2016. *Lancet Neurol.* **2018**, *17*, 939–953. [CrossRef] [PubMed]
2. Nichols, E.; Steinmetz, J.D.; Vollset, S.E.; Fukutaki, K.; Chalek, J.; Abd-Allah, F.; Abdoli, A.; Abualhasan, A.; Abu-Gharbieh, E.; Akram, T.T.; et al. Estimation of the Global Prevalence of Dementia in 2019 and Forecasted Prevalence in 2050: An Analysis for the Global Burden of Disease Study 2019. *Lancet Public Health* **2022**, *7*, e105–e125. [CrossRef] [PubMed]
3. Sun, H.; Saeedi, P.; Karuranga, S.; Pinkepank, M.; Ogurtsova, K.; Duncan, B.B.; Stein, C.; Basit, A.; Chan, J.C.N.; Mbanya, J.C.; et al. IDF Diabetes Atlas: Global, Regional and Country-Level Diabetes Prevalence Estimates for 2021 and Projections for 2045. *Diabetes Res. Clin. Pract.* **2022**, *183*, 109119. [CrossRef] [PubMed]
4. Karran, E.; De Strooper, B. The Amyloid Hypothesis in Alzheimer Disease: New Insights from New Therapeutics. *Nat. Rev. Drug Discov.* **2022**, *21*, 306–318. [CrossRef] [PubMed]
5. Alavi Naini, S.M.; Soussi-Yanicostas, N. Tau Hyperphosphorylation and Oxidative Stress, a Critical Vicious Circle in Neurodegenerative Tauopathies? *Oxid. Med. Cell. Longev.* **2015**, *2015*, 151979. [CrossRef] [PubMed]
6. Selkoe, D.; Hardy, J. The Amyloid Hypothesis of Alzheimer's Disease at 25 Years. *EMBO Mol. Med.* **2016**, *8*, 595–608. [CrossRef] [PubMed]
7. Stefanachi, A.; Leonetti, F.; Pisani, L.; Catto, M.; Carotti, A. Coumarin: A Natural, Privileged and Versatile Scaffold for Bioactive Compounds. *Molecules* **2018**, *23*, 250. [CrossRef] [PubMed]
8. Mishra, P.S.; Kumar, A.; Kaur, K.; Jaitak, V. Recent Developments in Coumarin Derivatives as Neuroprotective Agents. *Curr. Med. Chem.* **2024**, *31*, 5702–5738. [CrossRef] [PubMed]
9. Soto-Ortega, D.D.; Murphy, B.P.; Gonzalez-Velasquez, F.J.; Wilson, K.A.; Xie, F.; Wang, Q.; Moss, M.A. Inhibition of Amyloid-β Aggregation by Coumarin Analogs Can Be Manipulated by Functionalization of the Aromatic Center. *Bioorg. Med. Chem.* **2011**, *19*, 2596–2602. [CrossRef] [PubMed]
10. Rajasekhar, K.; Narayanaswamy, N.; Murugan, N.A.; Kuang, G.; Ågren, H.; Govindaraju, T. A High Affinity Red Fluorescence and Colorimetric Probe for Amyloid β Aggregates. *Sci. Rep.* **2016**, *6*, 23668. [CrossRef] [PubMed]
11. Gazit, E. A Possible Role for Pi-Stacking in the Self-Assembly of Amyloid Fibrils. *FASEB J.* **2002**, *16*, 77–83. [CrossRef] [PubMed]
12. Profit, A.A.; Felsen, V.; Chinwong, J.; Mojica, E.-R.E.; Desamero, R.Z.B. Evidence of π-Stacking Interactions in the Self-Assembly of hIAPP22–29. *Proteins* **2013**, *81*, 690–703. [CrossRef] [PubMed]
13. Rohani Sarvestani, Z.; Hashemi, M.; Solati, Z. π-Stacking Interactions between Curcumin and Aromatic Ring of Amino Acids in Amyloid Fibrils: A Theoretical Study. *Comput. Theor. Chem.* **2023**, *1225*, 114175. [CrossRef]
14. Biancalana, M.; Koide, S. Molecular Mechanism of Thioflavin-T Binding to Amyloid Fibrils. *Biochim. Biophys. Acta (BBA)-Proteins Proteom.* **2010**, *1804*, 1405–1412. [CrossRef] [PubMed]

15. Annunziata, F.; Pinna, C.; Dallavalle, S.; Tamborini, L.; Pinto, A. An Overview of Coumarin as a Versatile and Readily Accessible Scaffold with Broad-Ranging Biological Activities. *Int. J. Mol. Sci.* **2020**, *21*, 4618. [CrossRef] [PubMed]
16. Prasad, S.; Tyagi, A.K.; Aggarwal, B.B. Recent Developments in Delivery, Bioavailability, Absorption and Metabolism of Curcumin: The Golden Pigment from Golden Spice. *Cancer Res. Treat.* **2014**, *46*, 2–18. [CrossRef] [PubMed]
17. Zeb, Z.; Sharif, A.; Akhtar, B.; Shahnaz. 3-Acetyl Coumarin Alleviate Neuroinflammatory Responses and Oxidative Stress in Aluminum Chloride-Induced Alzheimer's Disease Rat Model. *Inflammopharmacology* **2024**, *32*, 1371–1386. [CrossRef] [PubMed]
18. Lewis, D.F.V.; Ito, Y.; Lake, B.G. Metabolism of Coumarin by Human P450s: A Molecular Modelling Study. *Toxicol. Vitr.* **2006**, *20*, 256–264. [CrossRef] [PubMed]
19. Foroozesh, M.; Sridhar, J.; Goyal, N.; Liu, J. Coumarins and P450s, Studies Reported to-Date. *Molecules* **2019**, *24*, 1620. [CrossRef] [PubMed]
20. Menon, S.; Armstrong, S.; Hamzeh, A.; Visanji, N.P.; Sardi, S.P.; Tandon, A. Alpha-Synuclein Targeting Therapeutics for Parkinson's Disease and Related Synucleinopathies. *Front. Neurol.* **2022**, *13*, 852003. [CrossRef] [PubMed]
21. Xiao, Y.; Ma, B.; McElheny, D.; Parthasarathy, S.; Long, F.; Hoshi, M.; Nussinov, R.; Ishii, Y. Aβ(1–42) Fibril Structure Illuminates Self-Recognition and Replication of Amyloid in Alzheimer's. *Nat. Struct. Mol. Biol.* **2015**, *22*, 499–505. [CrossRef] [PubMed]
22. Furkan, M.; Qais, F.A.; Khan, M.S.; Khan, M.R.; Ahmad, I.; Khan, R.H. Coumarin Prevents the Oligomerization and Aggregation of Amyloid β: Deciphering the Mode of Action Using Molecular Simulations. *J. Comput. Biophys. Chem.* **2025**, *24*, 781–794. [CrossRef]
23. Takomthong, P.; Waiwut, P.; Yenjai, C.; Sripanidkulchai, B.; Reubroycharoen, P.; Lai, R.; Kamau, P.; Boonyarat, C. Structure–Activity Analysis and Molecular Docking Studies of Coumarins from Toddalia Asiatica as Multifunctional Agents for Alzheimer's Disease. *Biomedicines* **2020**, *8*, 107. [CrossRef] [PubMed]
24. Yusufzai, S.K.; Khan, M.S.; Sulaiman, O.; Osman, H.; Lamjin, D.N. Molecular Docking Studies of Coumarin Hybrids as Potential Acetylcholinesterase, Butyrylcholinesterase, Monoamine Oxidase A/B and β-Amyloid Inhibitors for Alzheimer's Disease. *Chem. Cent. J.* **2018**, *12*, 128. [CrossRef] [PubMed]
25. Hamuľaková, S.; Gucký, A.; Mezencev, R.; Kožurková, M.; Bednáriková, Z.; Marek, J.; Soukup, O.; Janoušek, J.; Gažová, Z. Inhibition of Amyloid Fibrillization of Amyloid β Peptide by 4,7-Disubstituted Coumarin Derivatives. *Bioorg. Med. Chem.* **2025**, *129*, 118302. [CrossRef] [PubMed]
26. Kumar, S.; Kumar, M.; Tyagi, Y.K.; Kumar, S. Inhibition of Amyloid Fibrillation of HEWL by 4-Methylcoumarin and 4-Methylthiocoumarin Derivatives. *Curr. Pharm. Biotechnol.* **2021**, *22*, 232–244. [CrossRef] [PubMed]
27. Naz, N.; Nazli, Z.-H.; Parveen, S.; Shafiq, N. De Novo Drug Design, Synthesis, Biological Evaluation, and Structural Examination of Novel Coumarin-Based Pyrimidine Co-Drugs Accompanied by Molecular Docking and DFT Studies. *ACS Omega* **2026**, *11*, 15233–15253. [CrossRef] [PubMed]
28. Parvej, H.; Begum, S.; Dalui, R.; Paul, S.; Mondal, B.; Sardar, S.; Sepay, N.; Maiti, G.; Chandra Halder, U. Coumarin Derivatives Inhibit the Aggregation of β-Lactoglobulin. *RSC Adv.* **2022**, *12*, 17020–17028. [CrossRef] [PubMed]
29. Ademoye, T.A.; Ganegamage, S.K.; Masoudi, B.; Ibrahium, O.M.H.; Alnakhala, H.; Tripathi, A.; Dettmer, U.; Ostafe, R.; Borhan, B.; Fortin, J.S. In Vitro Evaluation of Amide-Linked Coumarin Scaffolds for the Inhibition of α-Synuclein and Tau Aggregation. *ACS Omega* **2025**, *10*, 38498–38514. [CrossRef] [PubMed]
30. Ranade, D.S.; Bapat, A.M.; Ramteke, S.N.; Joshi, B.N.; Roussel, P.; Tomas, A.; Deschamps, P.; Kulkarni, P.P. Thiosemicarbazone Modification of 3-Acetyl Coumarin Inhibits Aβ Peptide Aggregation and Protect against Aβ-Induced Cytotoxicity. *Eur. J. Med. Chem.* **2016**, *121*, 803–809. [CrossRef] [PubMed]
31. Huang, M.; Xie, S.-S.; Jiang, N.; Lan, J.-S.; Kong, L.-Y.; Wang, X.-B. Multifunctional Coumarin Derivatives: Monoamine Oxidase B (MAO-B) Inhibition, Anti-β-Amyloid (Aβ) Aggregation and Metal Chelation Properties against Alzheimer's Disease. *Bioorg. Med. Chem. Lett.* **2015**, *25*, 508–513. [CrossRef] [PubMed]
32. Rullo, M.; Spada, G.L.; Stefanachi, A.; Macchia, E.; Pisani, L.; Leonetti, F. Playing Around the Coumarin Core in the Discovery of Multimodal Compounds Directed at Alzheimer's-Related Targets: A Recent Literature Overview. *Molecules* **2025**, *30*, 891. [CrossRef] [PubMed]
33. Masroor, A.; Chandel, T.I.; Malik, S.; Mateen, Q.N.; Uversky, V.N.; Khan, R.H. Evaluation of ThT Augmentation and RLS Inner Filter Effect Caused by Highly Fluorescent Coumarin Derivative and Establishing It as True Inhibitor of Amyloid Fibrillation. *Arch. Biochem. Biophys.* **2021**, *709*, 108981. [CrossRef] [PubMed]
34. Xue, C.; Lin, T.Y.; Chang, D.; Guo, Z. Thioflavin T as an Amyloid Dye: Fibril Quantification, Optimal Concentration and Effect on Aggregation. *R. Soc. Open Sci.* **2017**, *4*, 160696. [CrossRef] [PubMed]
35. Liu, W.; Wu, L.; Liu, W.; Tian, L.; Chen, H.; Wu, Z.; Wang, N.; Liu, X.; Qiu, J.; Feng, X.; et al. Design, Synthesis and Biological Evaluation of Novel Coumarin Derivatives as Multifunctional Ligands for the Treatment of Alzheimer's Disease. *Eur. J. Med. Chem.* **2022**, *242*, 114689. [CrossRef] [PubMed]
36. Yang, A.; Zhang, H.; Hu, C.; Wang, X.; Shen, R.; Kou, X.; Wang, H. Novel Coumarin Derivatives as Multifunctional Anti-AD Agents: Design, Synthesis, X-Ray Crystal Structure and Biological Evaluation. *J. Mol. Struct.* **2022**, *1268*, 133747. [CrossRef]

37. Kamel, N.N.; Aly, H.F.; Fouad, G.I.; El-Karim, S.S.A.; Anwar, M.M.; Syam, Y.M.; Elseginy, S.A.; Ahmed, K.A.; Booles, H.F.; Shalaby, M.B.; et al. Anti-Alzheimer Activity of New Coumarin-Based Derivatives Targeting Acetylcholinesterase Inhibition. *RSC Adv.* **2023**, *13*, 18496–18510. [CrossRef] [PubMed]
38. Huang, C.-C.; Chang, K.-H.; Chiu, Y.-J.; Chen, Y.-R.; Lung, T.-H.; Hsieh-Li, H.M.; Su, M.-T.; Sun, Y.-C.; Chen, C.-M.; Lin, W.; et al. Multi-Target Effects of Novel Synthetic Coumarin Derivatives Protecting Aβ-GFP SH-SY5Y Cells against Aβ Toxicity. *Cells* **2021**, *10*, 3095. [CrossRef] [PubMed]
39. Boulaamane, Y.; Ahmad, I.; Patel, H.; Das, N.; Britel, M.R.; Maurady, A. Structural Exploration of Selected C6 and C7-Substituted Coumarin Isomers as Selective MAO-B Inhibitors. *J. Biomol. Struct. Dyn.* **2023**, *41*, 2326–2340. [CrossRef] [PubMed]
40. Sharmah, H.; Ahmed, L.A.; Kemisetti, D.; Kumar, S.; Samanthula, K.S.; Panigrahy, U.P.; Ghosh, N.S. Current Advances in 7-Hydroxycoumarin Derivatives as Potential Therapeutic Agents for Alzheimer's Disease. *Mol. Divers.* **2026**. [CrossRef] [PubMed]
41. Dvir, H.; Silman, I.; Harel, M.; Rosenberry, T.L.; Sussman, J.L. Acetylcholinesterase: From 3D Structure to Function. *Chem.-Biol. Interact.* **2010**, *187*, 10–22. [CrossRef] [PubMed]
42. Kowalczyk, P.; Koszelewski, D.; Misztal, T.; Szlis, M.; Młotkowska, P.; Gołębiewski, M.; Głowacz, K.; Kocot, M.; Marczyk, M.; Wypych, A.; et al. Blood–Brain Barrier Penetration of Novel 4-Trifluoromethyl-Coumarin Hybrids with Antibacterial Properties as Potential Brain Therapeutics in the Context of Spatially Diverse Healthcare Systems. *Int. J. Mol. Sci.* **2025**, *26*, 9655. [CrossRef] [PubMed]
43. Babaei, E.; Küçükkılınç, T.T.; Jalili-Baleh, L.; Nadri, H.; Öz, E.; Forootanfar, H.; Hosseinzadeh, E.; Akbari, T.; Ardestani, M.S.; Firoozpour, L.; et al. Novel Coumarin–Pyridine Hybrids as Potent Multi-Target Directed Ligands Aiming at Symptoms of Alzheimer's Disease. *Front. Chem.* **2022**, *10*, 895483. [CrossRef] [PubMed]
44. Bhatia, R.; Chakrabarti, S.S.; Kaur, U.; Parashar, G.; Banerjee, A.; Rawal, R.K. Multi-Target Directed Ligands (MTDLs): Promising Coumarin Hybrids for Alzheimer's Disease. *Curr. Alzheimer Res.* **2021**, *18*, 802–830. [CrossRef] [PubMed]
45. Jin, X.; Wang, Y.; Li, X.; Tan, X.; Miao, Z.; Chen, Y.; Hamdy, R.C.; Chua, B.H.L.; Kong, J.; Zhao, H.; et al. 7,8-Dihydroxy-4-Methylcoumarin Provides Neuroprotection by Increasing Hippocalcin Expression. *Neurotox. Res.* **2015**, *27*, 268–274. [CrossRef] [PubMed]
46. Sharma, A.; Bharate, S.B. Synthesis and Biological Evaluation of Coumarin Triazoles as Dual Inhibitors of Cholinesterases and β-Secretase. *ACS Omega* **2023**, *8*, 11161–11176. [CrossRef] [PubMed]
47. Li, S.; Li, X.; Li, S.; Chen, D.; Xia, C. Discovery of Novel Hybrids of Coumarin and Quinoline as Potential Anti-Alzheimer's Disease Agent. *Bioorg. Med. Chem.* **2026**, *133*, 118499. [CrossRef] [PubMed]
48. Wang, Z.-P.; Zhang, W.; Xing, L.-Z.; Zhao, Y.-D.; Xu, J.; Zhang, Y.-X. Therapeutic Potential of Coumarin-Polyphenolic Acid Hybrids in PD: Inhibition of α-Syn Aggregation and Disaggregation of Preformed Fibrils, Leading to Reduced Neuronal Inclusion Formation. *Bioorg. Med. Chem. Lett.* **2024**, *99*, 129618. [CrossRef] [PubMed]
49. Abd El-Mageed, M.M.A.; Fattah Ezzat, M.A.; Moussa, S.A.; Abdel-Aziz, H.A.; Elmasry, G.F. Rational Design, Synthesis and Computational Studies of Multi-Targeted Anti-Alzheimer's Agents Integrating Coumarin Scaffold. *Bioorg. Chem.* **2025**, *154*, 108024. [CrossRef] [PubMed]
50. Pisani, L.; Catto, M.; Muncipinto, G.; Nicolotti, O.; Carrieri, A.; Rullo, M.; Stefanachi, A.; Leonetti, F.; Altomare, C. A Twenty-Year Journey Exploring Coumarin-Based Derivatives as Bioactive Molecules. *Front. Chem.* **2022**, *10*, 1002547. [CrossRef] [PubMed]
51. Husain, A.; AI Balushi, K.; Akhtar, M.J.; Khan, S.A. Coumarin Linked Heterocyclic Hybrids: A Promising Approach to Develop Multi Target Drugs for Alzheimer's Disease. *J. Mol. Struct.* **2021**, *1241*, 130618. [CrossRef]
52. Pourabdi, L.; Küçükkılınç, T.T.; Khoshtale, F.; Ayazgök, B.; Nadri, H.; Farokhi Alashti, F.; Forootanfar, H.; Akbari, T.; Shafiei, M.; Foroumadi, A.; et al. Synthesis of New 3-Arylcoumarins Bearing N-Benzyl Triazole Moiety: Dual Lipoxygenase and Butyrylcholinesterase Inhibitors with Anti-Amyloid Aggregation and Neuroprotective Properties Against Alzheimer's Disease. *Front. Chem.* **2022**, *9*, 810233. [CrossRef] [PubMed]
53. Lin, T.-H.; Chang, K.-H.; Chiu, Y.-J.; Weng, Z.-K.; Sun, Y.-C.; Lin, W.; Lee-Chen, G.-J.; Chen, C.-M. Neuroprotective Action of Coumarin Derivatives through Activation of TRKB-CREB-BDNF Pathway and Reduction of Caspase Activity in Neuronal Cells Expressing Pro-Aggregated Tau Protein. *Int. J. Mol. Sci.* **2022**, *23*, 12734. [CrossRef] [PubMed]
54. Chiu, Y.-J.; Lin, T.-H.; Chen, C.-M.; Lin, C.-H.; Teng, Y.-S.; Lin, C.-Y.; Sun, Y.-C.; Hsieh-Li, H.M.; Su, M.-T.; Lee-Chen, G.-J.; et al. Novel Synthetic Coumarin-Chalcone Derivative (E)-3-(3-(4-(Dimethylamino)Phenyl)Acryloyl)-4-Hydroxy-2H-Chromen-2-One Activates CREB-Mediated Neuroprotection in Aβ and Tau Cell Models of Alzheimer's Disease. *Oxidative Med. Cell. Longev.* **2021**, *2021*, 3058861. [CrossRef] [PubMed]
55. Berrino, E.; Carradori, S.; Carta, F.; Melfi, F.; Gallorini, M.; Poli, G.; Tuccinardi, T.; Fernández-Bolaños, J.G.; López, Ó.; Petzer, J.P.; et al. A Multitarget Approach against Neuroinflammation: Alkyl Substituted Coumarins as Inhibitors of Enzymes Involved in Neurodegeneration. *Antioxidants* **2023**, *12*, 2044. [CrossRef] [PubMed]
56. Hassanein, E.H.M.; Sayed, A.M.; Hussein, O.E.; Mahmoud, A.M. Coumarins as Modulators of the Keap1/Nrf2/ARE Signaling Pathway. *Oxidative Med. Cell. Longev.* **2020**, *2020*, 1675957. [CrossRef] [PubMed]

57. Saadati, F.; Modarresi Chahardehi, A.; Jamshidi, N.; Jamshidi, N.; Ghasemi, D. Coumarin: A Natural Solution for Alleviating Inflammatory Disorders. *Curr. Res. Pharmacol. Drug Discov.* **2024**, *7*, 100202. [CrossRef] [PubMed]
58. Herbet, M.; Wicha-Komsta, K.; Pawłowski, K.; Bąk, E.; Sterczewski, P.; Hryć, B.; Walczak, Ł.; Skalicka-Woźniak, K.; Siedlaczek, W.; Gawrońska-Grzywacz, M.; et al. Behavioral, Neurochemical, and Biochemical Investigations of Coumarin Derivatives in Modulating Neuroinflammation, Cholinergic Dysfunction, and Cytokine Responses: In Vivo Studies for Potential Alzheimer's Disease Therapy. *Behav. Brain Res.* **2026**, *497*, 115891. [CrossRef] [PubMed]
59. Pardridge, W.M. Blood–Brain Barrier Delivery. *Drug Discov. Today* **2007**, *12*, 54–61. [CrossRef] [PubMed]
60. Cornelissen, F.M.G.; Markert, G.; Deutsch, G.; Antonara, M.; Faaij, N.; Bartelink, I.; Noske, D.; Vandertop, W.P.; Bender, A.; Westerman, B.A. Explaining Blood–Brain Barrier Permeability of Small Molecules by Integrated Analysis of Different Transport Mechanisms. *J. Med. Chem.* **2023**, *66*, 7253–7267. [CrossRef] [PubMed]
61. Sharma, A.; Nuthakki, V.K.; Gairola, S.; Singh, B.; Bharate, S.B. A Coumarin−Donepezil Hybrid as a Blood−Brain Barrier Permeable Dual Cholinesterase Inhibitor: Isolation, Synthetic Modifications, and Biological Evaluation of Natural Coumarins. *ChemMedChem* **2022**, *17*, e202200300. [CrossRef] [PubMed]
62. Daina, A.; Michielin, O.; Zoete, V. SwissADME: A Free Web Tool to Evaluate Pharmacokinetics, Drug-Likeness and Medicinal Chemistry Friendliness of Small Molecules. *Sci. Rep.* **2017**, *7*, 42717. [CrossRef] [PubMed]
63. Huang, E.T.C.; Yang, J.-S.; Liao, K.Y.K.; Tseng, W.C.W.; Lee, C.K.; Gill, M.; Compas, C.; See, S.; Tsai, F.-J. Predicting Blood–Brain Barrier Permeability of Molecules with a Large Language Model and Machine Learning. *Sci. Rep.* **2024**, *14*, 15844. [CrossRef] [PubMed]
64. Wager, T.T.; Hou, X.; Verhoest, P.R.; Villalobos, A. Central Nervous System Multiparameter Optimization Desirability: Application in Drug Discovery. *ACS Chem. Neurosci.* **2016**, *7*, 767–775. [CrossRef] [PubMed]
65. Fridén, M.; Bergström, F.; Wan, H.; Rehngren, M.; Ahlin, G.; Hammarlund-Udenaes, M.; Bredberg, U. Measurement of Unbound Drug Exposure in Brain: Modeling of pH Partitioning Explains Diverging Results between the Brain Slice and Brain Homogenate Methods. *Drug Metab. Dispos.* **2011**, *39*, 353–362. [CrossRef] [PubMed]
66. Di, L.; Kerns, E.H.; Fan, K.; McConnell, O.J.; Carter, G.T. High Throughput Artificial Membrane Permeability Assay for Blood-Brain Barrier. *Eur. J. Med. Chem.* **2003**, *38*, 223–232. [CrossRef] [PubMed]
67. Radan, M.; Djikic, T.; Obradovic, D.; Nikolic, K. Application of In Vitro PAMPA Technique and In Silico Computational Methods for Blood-Brain Barrier Permeability Prediction of Novel CNS Drug Candidates. *Eur. J. Pharm. Sci.* **2022**, *168*, 106056. [CrossRef] [PubMed]
68. Hubatsch, I.; Ragnarsson, E.G.E.; Artursson, P. Determination of Drug Permeability and Prediction of Drug Absorption in Caco-2 Monolayers. *Nat. Protoc.* **2007**, *2*, 2111–2119. [CrossRef] [PubMed]
69. Raaphorst, R.M.; Savolainen, H.; Cantore, M.; van de Steeg, E.; van Waarde, A.; Colabufo, N.A.; Elsinga, P.H.; Lammertsma, A.A.; Windhorst, A.D.; Luurtsema, G. Comparison of In Vitro Assays in Selecting Radiotracers for In Vivo P-Glycoprotein PET Imaging. *Pharmaceuticals* **2017**, *10*, 76. [CrossRef] [PubMed]
70. Banker, M.J.; Clark, T.H.; Williams, J.A. Development and Validation of a 96-Well Equilibrium Dialysis Apparatus for Measuring Plasma Protein Binding. *J. Pharm. Sci.* **2003**, *92*, 967–974. [CrossRef] [PubMed]
71. Thakur, A.; Tawa, G.J.; Henderson, M.J.; Danchik, C.; Liu, S.; Shah, P.; Wang, A.Q.; Dunn, G.; Kabir, M.; Padilha, E.C.; et al. Design, Synthesis, and Biological Evaluation of Quinazolin-4-One-Based Hydroxamic Acids as Dual PI3K/HDAC Inhibitors. *J. Med. Chem.* **2020**, *63*, 4256–4292. [CrossRef] [PubMed]
72. Walsky, R.L.; Obach, R.S. Validated Assays for Human Cytochrome P450 Activities. *Drug Metab. Dispos.* **2004**, *32*, 647–660. [CrossRef] [PubMed]
73. Shamsi, S.; Tran, H.; Tan, R.S.J.; Tan, Z.J.; Lim, L.Y. Curcumin, Piperine, and Capsaicin: A Comparative Study of Spice-Mediated Inhibition of Human Cytochrome P450 Isozyme Activities. *Drug Metab. Dispos.* **2017**, *45*, 49–55. [CrossRef] [PubMed]
74. Born, S.L.; Rodriguez, P.A.; Eddy, C.L.; Lehman-McKeeman, L.D. Synthesis and Reactivity of Coumarin 3,4-Epoxide. *Drug Metab. Dispos.* **1997**, *25*, 1318–1323. [PubMed]
75. Smith, Q.R.; Fisher, C.; Allen, D.D. The Role of Plasma Protein Binding in Drug Delivery to Brain. In *Blood—Brain Barrier: Drug Delivery and Brain Pathology*; Kobiler, D., Lustig, S., Shapira, S., Eds.; Springer: Boston, MA, USA, 2001; pp. 311–321.
76. Xia, X.; Zhou, Y.; Gao, H. Prodrug Strategy for Enhanced Therapy of Central Nervous System Disease. *Chem. Commun.* **2021**, *57*, 8842–8855. [CrossRef] [PubMed]
77. Tiseo, P.J.; Rogers, S.L.; Friedhoff, L.T. Pharmacokinetic and Pharmacodynamic Profile of Donepezil HCl Following Evening Administration. *Br. J. Clin. Pharmacol.* **1998**, *46*, 13–18. [CrossRef] [PubMed]
78. Farlow, M.R. Clinical Pharmacokinetics of Galantamine. *Clin. Pharmacokinet.* **2003**, *42*, 1383–1392. [CrossRef] [PubMed]
79. Matos, M.J. Coumarin and Its Derivatives—Editorial. *Molecules* **2021**, *26*, 6320. [CrossRef] [PubMed]
80. Paul, R.; Firdous, S.M. Unraveling the Molecular Mechanisms of Aluminium Chloride-Induced Alzheimer's Disease. *Biometals* **2026**, *39*, 539–564. [CrossRef] [PubMed]

81. Mehra, S.; Sahay, S.; Maji, S.K. α-Synuclein Misfolding and Aggregation: Implications in Parkinson's Disease Pathogenesis. *Biochim. Biophys. Acta (BBA)-Proteins Proteom.* **2019**, *1867*, 890–908. [CrossRef] [PubMed]
82. Das, S.; Pukala, T.L.; Smid, S.D. Exploring the Structural Diversity in Inhibitors of α-Synuclein Amyloidogenic Folding, Aggregation, and Neurotoxicity. *Front. Chem.* **2018**, *6*, 181. [CrossRef] [PubMed]
83. Pujols, J.; Peña-Díaz, S.; Lázaro, D.F.; Peccati, F.; Pinheiro, F.; González, D.; Carija, A.; Navarro, S.; Conde-Giménez, M.; García, J.; et al. Small Molecule Inhibits α-Synuclein Aggregation, Disrupts Amyloid Fibrils, and Prevents Degeneration of Dopaminergic Neurons. *Proc. Natl. Acad. Sci. USA* **2018**, *115*, 10481–10486. [CrossRef] [PubMed]
84. Elangovan, N.; Jayaraj, R.L.; Ranjani, V.; Manigandan, K. In Silico Docking Studies to Identify Potent Inhibitors of Alpha Synuclein Aggregation in Parkinson Disease. *Asian J. Pharm. Clin. Res.* **2013**, *6*, 127–131.
85. Alrouji, M.; Al-Kuraishy, H.M.; Al-Gareeb, A.I.; Alexiou, A.; Papadakis, M.; Saad, H.M.; Batiha, G.E.-S. The Potential Role of Human Islet Amyloid Polypeptide in Type 2 Diabetes Mellitus and Alzheimer's Diseases. *Diabetol. Metab. Syndr.* **2023**, *15*, 101. [CrossRef] [PubMed]
86. Weirich, F.; Gremer, L.; Mirecka, E.A.; Schiefer, S.; Hoyer, W.; Heise, H. Structural Characterization of Fibrils from Recombinant Human Islet Amyloid Polypeptide by Solid-State NMR: The Central FGAILS Segment Is Part of the β-Sheet Core. *PLoS ONE* **2016**, *11*, e0161243. [CrossRef] [PubMed]
87. Babu, P.R.; Turner, C.; Ryznar, R. Cross-Seeding of IAPP and Aβ42: A Review of the Molecular Link between Type 2 Diabetes and Alzheimer's Disease. *Metab. Brain Dis.* **2025**, *41*, 8. [CrossRef] [PubMed]
88. Cao, Q.; Boyer, D.R.; Sawaya, M.R.; Ge, P.; Eisenberg, D.S. Cryo-EM Structure and Inhibitor Design of Human IAPP (Amylin) Fibrils. *Nat. Struct. Mol. Biol.* **2020**, *27*, 653–659. [CrossRef] [PubMed]
89. Taylor, A.I.P.; Xu, Y.; Wilkinson, M.; Chakraborty, P.; Brinkworth, A.; Willis, L.F.; Zhuravleva, A.; Ranson, N.A.; Foster, R.; Radford, S.E. Kinetic Steering of Amyloid Formation and Polymorphism by Canagliflozin, a Type-2 Diabetes Drug. *J. Am. Chem. Soc.* **2025**, *147*, 11859–11878. [CrossRef] [PubMed]
90. Zeki, N.M.; Mustafa, Y.F. Coumarin Hybrids: A Sighting of Their Roles in Drug Targeting. *Chem. Pap.* **2024**, *78*, 5753–5772. [CrossRef]
91. Kowalczyk, J.; Skalicka-Wozniak, K.; Budzynska, B.; Sayed, N.E.; Espargaró, A.; Sabate, R. Coumarin Derivatives against Amyloid-Beta 40–42 Peptide Andtauprotein. *Curr. Issues Pharm. Med. Sci.* **2022**, *35*, 67–74. [CrossRef]